Original Article

MOLECULAR METABOLISM

Peptide-YY_{3-36}/glucagon-like peptide-1 combination treatment of obese diabetic mice improves insulin sensitivity associated with recovered pancreatic β-cell function and synergistic activation of discrete hypothalamic and brainstem neuronal circuitries

Brandon B. Boland [1,2,3,6], Rhianna C. Laker [1,2], Siobhan O'Brien [4,5], Sadichha Sitaula [1,2], Isabelle Sermadiras [4,5], Jens Christian Nielsen [3], Pernille Barkholt [3], Urmas Roostalu [3], Jacob Hecksher-Sørensen [3], Sara Rubek Sejthen [3], Ditte Dencker Thorbek [3], Arthur Suckow [1,2,7], Nicole Burmeister [4,5,8], Stephanie Oldham [1,2], Sarah Will [1,2], Victor G. Howard [1,2], Benji M. Gill [1,2], Philip Newton [4,5], Jacqueline Naylor [1,2], David C. Hornigold [1,2], Jotham Austin [9], Louise Lantier [10], Owen P. McGuinness [10], James L. Trevaskis [1,2,11], Joseph S. Grimsby [1,2], Christopher J. Rhodes [1,2,*]

ABSTRACT

Objective: Obesity-linked type 2 diabetes (T2D) is a worldwide health concern and many novel approaches are being considered for its treatment and subsequent prevention of serious comorbidities. Co-administration of glucagon like peptide 1 (GLP-1) and peptide YY_{3-36} (PYY_{3-36}) renders a synergistic decrease in energy intake in obese men. However, mechanistic details of the synergy between these peptide agonists and their effects on metabolic homeostasis remain relatively scarce.

Methods: In this study, we utilized long-acting analogues of GLP-1 and PYY_{3-36} (via Fc-peptide conjugation) to better characterize the synergistic pharmacological benefits of their co-administration on body weight and glycaemic regulation in obese and diabetic mouse models. Hyperinsulinemic-euglycemic clamps were used to measure weight-independent effects of Fc-PYY_{3-36} + Fc-GLP-1 on insulin action. Fluorescent light sheet microscopy analysis of whole brain was performed to assess activation of brain regions.

Results: Co-administration of long-acting Fc-IgG/peptide conjugates of Fc-GLP-1 and Fc-PYY_{3-36} (specific for PYY receptor-2 (Y2R)) resulted in profound weight loss, restored glucose homeostasis, and recovered endogenous β-cell function in two mouse models of obese T2D. Hyperinsulinemic-euglycemic clamps in C57BLKS/J *db/db* and diet-induced obese Y2R-deficient (Y2RKO) mice indicated Y2R is required for a weight-independent improvement in peripheral insulin sensitivity and enhanced hepatic glycogenesis. Brain cFos staining demonstrated distinct temporal activation of regions of the hypothalamus and hindbrain following Fc-PYY_{3-36} + Fc-GLP-1R agonist administration.

Conclusions: These results reveal a therapeutic approach for obesity/T2D that improved insulin sensitivity and restored endogenous β-cell function. These data also highlight the potential association between the gut–brain axis in control of metabolic homeostasis.

Keywords Diabetes; Obesity; Insulin sensitivity; Pancreatic β-cell; Hypothalamus; Glucagon-like peptide-1 (GLP-1); Peptide-YY_{3-36} (PYY_{3-36}); Diabetes remission; Central nervous system; Glucose homeostasis

[1]Research and Early Development, Cardiovascular, Renal and Metabolism, BioPharmaceuticals R&D, AstraZeneca, Gaithersburg, MD, USA [2]Research and Early Development, Cardiovascular, Renal and Metabolism, BioPharmaceuticals R&D, AstraZeneca, Cambridge, UK [3]Gubra ApS, Horsholm, Denmark [4]Antibody and Protein Engineering, BioPharmaceuticals R&D, AstraZeneca, Gaithersburg, MD, USA [5]Antibody and Protein Engineering, BioPharmaceuticals R&D, AstraZeneca, Cambridge, UK [6]PRECISIONscientia, Yardley, PA, USA [7]DTX Pharma, San Diego, CA, USA [8]Roche, Penzberg, Germany [9]University of Chicago Advanced Electron Microscopy Core Facility, Chicago, IL, USA [10]Vanderbilt University Mouse Metabolic Phenotyping Center, Nashville, TN, USA [11]Gilead Sciences, Foster City, CA, USA

*Corresponding author. Cardiovascular, Renal and Metabolism, Biopharmaceuticals R&D, AstraZeneca Plc, One Medimmune Way, Gaithersburg, MD, 20878, USA. E-mail: christopher.rhodes@astrazeneca.com (C.J. Rhodes).

Received July 22, 2021 • Revision received October 22, 2021 • Accepted November 4, 2021 • Available online 12 November 2021

https://doi.org/10.1016/j.molmet.2021.101392

1. INTRODUCTION

Obesity is a pandemic affecting nearly two billion people who also have a significantly increased risk of comorbidities like type 2 diabetes (T2D) and its complications, cardiovascular disease, and several cancers worldwide [1]. Weight loss through lifestyle, diet, and behavioural modification has poor compliance, with the vast majority of patients relapsing in only a few years [2]. Conversely, bariatric surgeries, such as Roux-en-Y gastric bypass (RYGB), confer sustained weight loss and diabetes resolution [3,4]. However, bariatric surgery is not a scalable solution to address the ever-increasing obesity burden. Therefore, the need for effective pharmacotherapies has driven intense investigation into the molecular mechanisms underlying the efficacy of the surgical intervention, revealing several complex translatable possibilities, namely the postprandial increase in circulating gut-derived hormones [5].

Glucagon-like peptide 1 (GLP-1), derived from differential proteolytic processing of proglucagon, and PYY_{3-36}, generated by specific proteolysis of proPYY, are together secreted from intestinal epithelial endocrine L-cells in response to nutrient intake. Both hormones have emerged as leading pharmacological candidates for their potent physiological effects to reduce food intake and induce weight loss [6]. GLP-1 mediated activation of GLP-1 receptors (GLP-1R) on pancreatic β-cells potentiates glucose-induced insulin secretion and maintains β-cell mass. Central activation of GLP-1Rs, particularly in the hypothalamus and hindbrain, results in delayed gastric emptying as well as inhibition of food intake, that when pharmacological GLP-1 analogues are applied can drive clinically relevant weight loss [7,8]. The effects of PYY_{3-36} have almost exclusively been linked to central activation. PYY_{3-36} can reduce food intake in both rodents and man, and is thought to act via activation of the Neuropeptide Y Receptor Y2 (NPY2R) in the hypothalamus [9,10]. Overall, acute co-administration of PYY_{3-36} and GLP-1-derived peptides render a synergistic decrease in energy intake in obese individuals [11]. However, mechanistic details of the synergy between these peptide agonists beyond food intake, body weight control, and consequential effects on metabolic homeostasis remain relatively undefined. In the current study, we utilized long-acting analogues of GLP-1 and PYY_{3-36} (via Fc-peptide conjugation) with submaximal doses to better characterize the synergistic pharmacological benefits of their co-administration on body weight and glycaemic regulation in obese diabetic mouse models, and better outline the central neuronal circuitries by which they mediate these effects.

2. MATERIAL AND METHODS

2.1. Compounds and cAMP accumulation assay

IgG1 Fc was generated with a cysteine substitution at position 442 (442C) in the CH3 domain using standard DNA recombinant technologies [12] and expressed in Chinese Hamster Ovary (CHO) cells. The Y2R-selective peptide was prepared by automated solid-phase synthesis using the Fmoc/^{t}Bu protocol with a maleimide group at lysine 11 to enable conjugation of the peptide to the free Cys (442C) in the Fc molecule. Crude peptides were isolated by chromatography using an Agilent Polaris C8-A stationary phase (21.2 × 250 mm, 5 microns) eluting with a linear solvent gradient from 10% to 70% MeCN (0.1% TFA v/v) in water for 30 min using a Varian SD-1 Prep Star binary pump system, monitoring by UV absorption at 210 nm. Following reduction and oxidation, the Fc was site-specifically conjugated with the maleimide-functionalized PYY_{3-36} to yield Fc-PYY_{3-36} (Figure 1C). The Fc-GLP-1R agonist was an internally-generated (AstraZeneca, Gaithersburg, MD) version of Dulaglutide IgG4 Fc (same primary sequence) and purified as per Fc-PYY_{3-36}. Stable CHO cell lines overexpressing human or mouse GLP-1R, NPY2R, and human NPY1R, NPY4R or NPY5R were generated at AstraZeneca using public-domain-determined and -confirmed sequences for each receptor. Half-maximal agonist potency determinations (EC_{50}) for peptides inducing

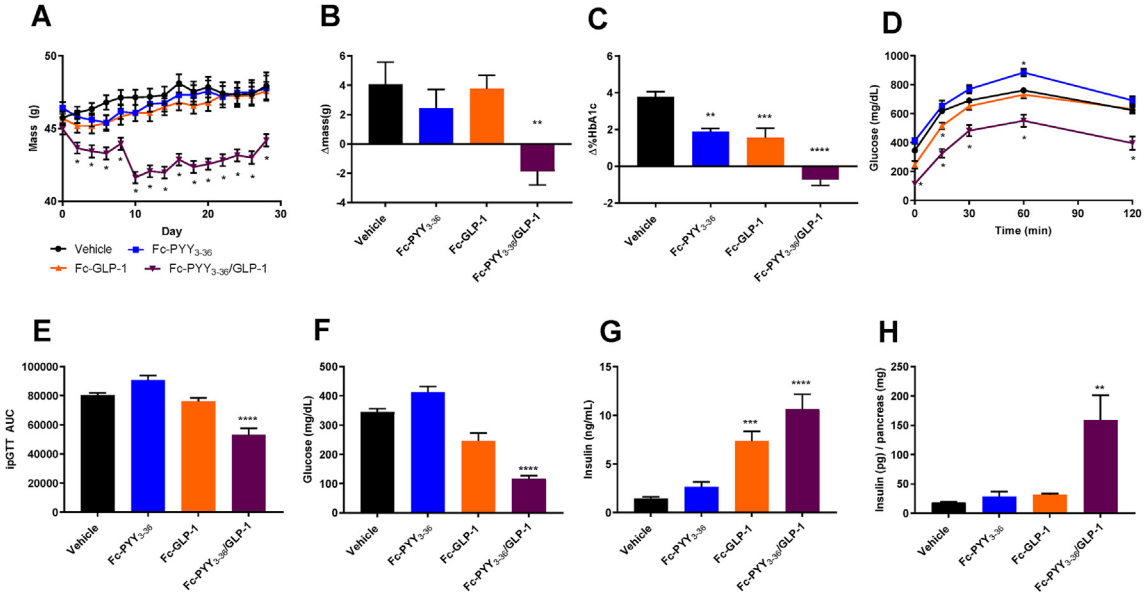

Figure 1: Physiological parameters of male KS *db/db* mice administered Fc-PYY_{3-36} (1 mg/kg), Fc-GLP-1 agonist (0.15 mg/kg) or Fc-PYY_{3-36}/GLP-1 agonist combination (1 mg/kg/0.15 mg/kg). A) Body weight profile of 8-week old animals during the 4-week treatment period. B) Change in body mass following 4 weeks of treatment (N = 20 for all groups). C) Change in %hbA1c following 4 weeks of treatment. N = 8 for all groups D) 6-hour fasted ipGTT (2g/kg) and E) associated AUC after 3 weeks of treatment. F) Fasting plasma glucose and G) fasting plasma insulin following 3 weeks of treatment, N = 12 for all groups. H) Pancreatic insulin content at study termination, N = 4 for all groups. $*p \leq 0.05$ vs Vehicle, $**p \leq 0.01$ vs Vehicle, $***p \leq 0.001$ vs Vehicle, $****p \leq 0.0001$ vs Vehicle.

cyclic adenosine monophosphate (cAMP) production were determined in the presence of 0.1% BSA (Figure 2). cAMP generation was measured using the CisBio dynamic d2 cAMP HTRF Assay kit (CisBio, Codolet, France) as per the manufacturer's protocol [13,14]. Cisplatin was purchased from Tocris Bioscience (Bristol, UK).

2.2. Experimental design

All animal studies were approved, as applicable, by either the Institutional Animal Care and Use Committee at MedImmune/AstraZeneca (Gaithersburg, MD, USA) or Vanderbilt University (Nashville, TN, USA) in accordance with Animal Welfare Act guidelines, or Gubra (Hørsholm, Denmark) under personal licenses issued by the Danish Committee for Animal Research. Eight cohorts of group-housed male mice were used in the current study. Cohort A consisted of 8-week old C57BLKS/J *db/db* mice (Jackson Labs, Bar Harbor, ME) used to assess the effects of Fc-GLP-1, Fc-PYY$_{3-36}$, and Fc-PYY$_{3-36}$ + Fc-GLP-1 on physiological parameters and β-cell function. Cohort B consisted of 8-week old C57BLKS/J *db/db* mice (Jackson Labs) used to assess the effect of Fc-PYY$_{3-36}$ + Fc-GLP-1 on energy expenditure and activity. Cohort C consisted of 9-week old C57BLKS/J *db/db* and *db/+* mice (Jackson Labs) used to assess the effect of Fc-PYY$_{3-36}$ + Fc-GLP-1 on insulin sensitivity and glucose disposal. Cohorts A-C were fed normal chow *ad libitum* before and during the experiment, except in experiments including weight-matched groups. In B and C cohorts, weight matching was achieved in C57BLKS/J *db/db* by pair feeding to match that consumed by the mice administered Fc-PYY$_{3-36}$/GLP-1 the previous day and, if required, further reducing the pair-fed amount by 5%–15% to maintain weight matching to the Fc-PYY$_{3-36}$/GLP-1 group. Cohort D consisted of high-fat diet-fed (Research Diets D12492, 8 weeks on diet) 18-week-old C57BL6/J and Y2RKO mice (Jackson Labs, Bar Harbor, ME, USA) used to assess the effect of Fc-PYY$_{3-36}$ + Fc-GLP-1 on insulin sensitivity and glucose disposal. Constitutive Y2RKO mice (C57BL/6NTac-Npy2r^{em3978Tac}; Y2RKO) were generated at Taconic (San Diego, CA) as described previously [15]. Cohort E consisted of 8-week old lean C57BL6/J, Y2RKO, and Y2RKO/GLP-1RKO double knockout mice (Janvier Labs and Taconic [16], that were used to assess the acute effect of IP-injected Fc-GLP-1, Fc-PYY$_{3-36}$, and Fc-PYY$_{3-36}$ + Fc-GLP-1 combination on central cFOS reactivity 4 h post-dose. Cohort F consisted of 8-week old lean C57BL6/J mice (Janvier Labs, France) used to assess the acute effect of IP-injected Fc-PYY$_{3-36}$ + Fc-GLP-1 on gene expression changes in the Area Postrema (AP), Nucleus Tractus Solitarius (NTS), and ParaVentricular Nucleus (PVN) brain regions 4 h post-dose. Cohort G consisted of 8-week-old lean C57BL6/J mice (Janvier Labs) used to assess the acute effect of IP-injected Fc-GLP-1, Fc-PYY$_{3-36}$, and Fc-PYY$_{3-36}$ + Fc-GLP-1 on whole-brain cFOS reactivity 24-h post-dose. Cohort H consisted of 8-

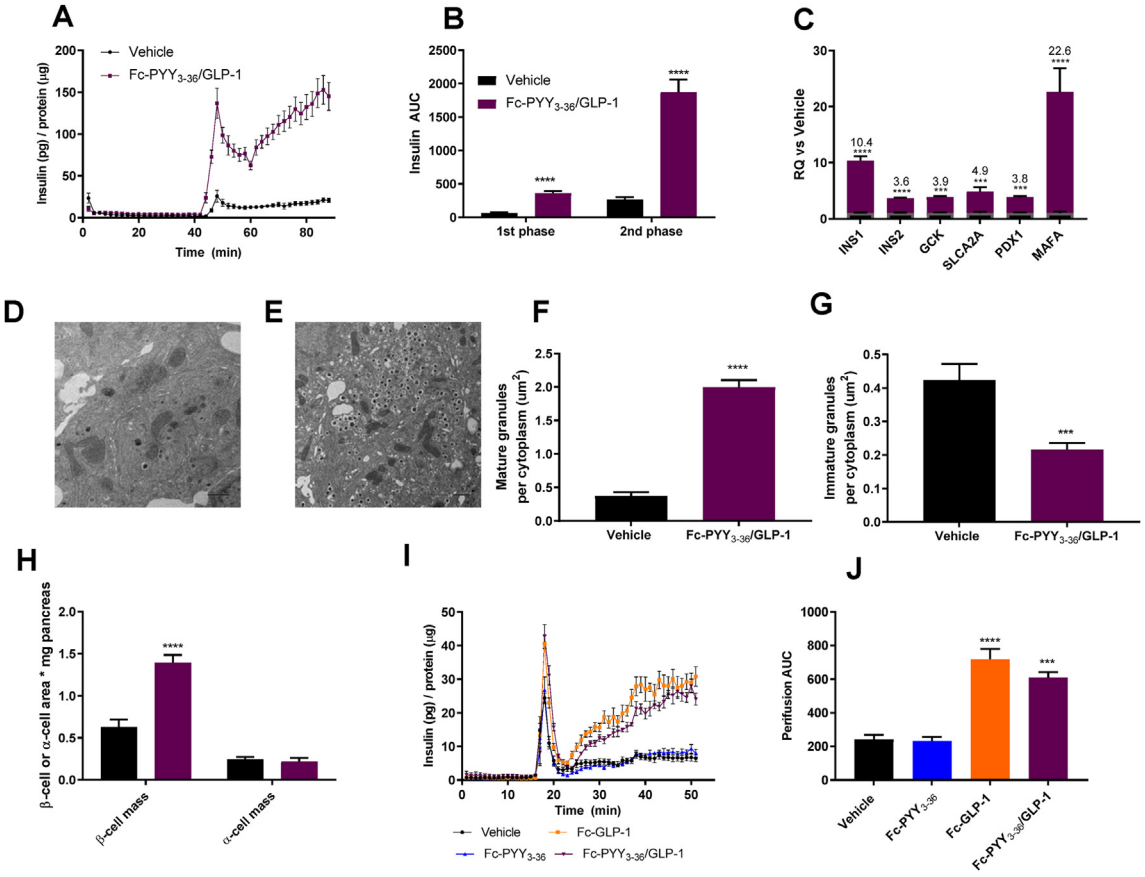

Figure 2: Effect of 4 week Fc-PYY$_{3-36}$/GLP-1 (1 mg/kg/0.15 mg/kg) combination treatment on β-cell function in KS *db/db* mice. A) Perifusion of freshly isolated islets and B) 1st and 2nd phase perifusion AUC; N = 4–5. C) Freshly isolated islet RT-qPCR for *Ins1, Ins2, Gck, Slca2a, Pdx1,* and *Mafa*. *Rna 18s* used as housekeeping. Data presented as relative expression versus vehicle. N = 5–6. D) Representative transmission electron micrograph of islets isolated from Vehicle and E) combination-treated animals. F) Quantification of mature insulin granules and G) immature insulin granules per total cytoplasmic area. N = 3–4 from >10 representative electron micrographs. H) β/α-cell mass from insulin/glucagon dual-stained immunohistochemistry sections. N = 3–4. I) Effect of Fc-PYY$_{3-36}$, Fc-GLP-1, and the combination on overnight cultured C57BL/6 J islet insulin secretion and the J) associated insulin AUC. N ≥ 3. ***$p \leq 0.001$ vs Vehicle, ****$p \leq 0.0001$ vs Vehicle.

week-old lean C57BL6/J mice (Janvier Labs) used to assess conditioned taste aversion to IP-injected Fc-GLP-1, Fc-PYY_{3-36}, and Fc-PYY_{3-36} + Fc-GLP-1. All cohorts were acclimatized for at least one week prior to study start. Cohorts A and B were randomized into groups based on haemoglobin A1c levels (%HbA1c), while all other cohorts were randomized based on body weight. Cohorts A, B, C, and D received Fc-GLP-1 (0.15 mg/kg SC, QAD), Fc-PYY_{3-36} (1.0 mg/kg SC, QAD), or Fc-PYY_{3-36} + Fc-GLP-1 (0.3 mg/kg/0.05 mg/kg SC, QAD dose-escalated to 1.0 mg/kg/0.15 mg/kg after one week). Cohorts E and F received Fc-GLP-1 (0.15 mg/kg IP), Fc-PYY_{3-36} (1.0 mg/kg IP), or Fc-PYY_{3-36} + Fc-GLP-1 (1.0 mg/kg/0.15 mg/kg IP) as indicated. Cohort G received Fc-GLP-1 (0.5 mg/kg IP), Fc-PYY_{3-36} (1.0 mg/kg IP), or Fc-PYY_{3-36} + Fc-GLP-1 (1.0 mg/kg/0.5 mg/kg IP) as indicated. Cohort H received Fc-GLP-1 (0.15 mg/kg SC), Fc-PYY_{3-36} (1.0 mg/kg SC), Fc-PYY_{3-36} + Fc-GLP-1 (1.0 mg/kg/0.15 mg/kg SC), or cisplatin (3 mg/kg SC). Phosphate-buffered saline (PBS) was used as the Vehicle control for all cohorts.

2.3. Intraperitoneal glucose tolerance test (ipGTT) and assay

Six-hour fasted mice were injected intraperitoneally with 2.0 g/kg glucose in saline. Blood glucose was determined at 0, 15, 30, 60, and 120 min. Plasma glucose was determined colourimetrically using a glucose oxidase kit (Cayman Chemical, Ann Arbor, MI). Plasma insulin levels were determined via ELISA (MesoScale Discovery, Rockville, MD) in cohort A, and via RIA (MilliporeSigma, Temecula, CA) in C and D cohorts. The haemoglobin A1c (HbA1c) level was determined colourimetrically from whole blood (Crystal Chem Inc, Elk Grove Village, IL, USA).

2.4. Islet and pancreas analysis

Pancreatic insulin content was determined from the whole pancreas using acid-ethanol extraction and insulin ELISA. For immunohistochemistry, pancreata were fixed, embedded, and cut into 5 μm long sections. Insulin and glucagon staining, quantitation, and analysis were all performed, as previously described [17,18]. Pancreatic islets from C57BL6/J or C57BLKS/J *db/db* mice were isolated by collagenase digestion, as previously described [19]. For quantitative real-time polymerase chain reaction (qRT-PCR) and transmission electron microscopy, freshly isolated islets from C57BLKS/J *db/db* mice were used. Transmission electron microscopy and quantitation of insulin secretory granule numbers were performed, as previously described [20]. qRT-PCR analysis was performed using Taqman gene expression assay probe/primer sets (Thermo Fischer Scientific, USA) for *Ins1, Ins2, Gck, Pdx1, Slca2a,* and *Rna18s.* PrimePCR Probe Assay (Bio-Rad, Hercules, CA) was used for *Mafa.* Results are shown as the target gene expression relative to *Rna18s* expression and normalized to vehicle expression using the $2^{(-\Delta\Delta Ct)}$ method. For perifusion, freshly isolated islets from C57BLKS/J *db/db* mice (Figure 2A–B) or overnight recovered islets (RPMI media, 10% FBS, 5.6 mmol/L glucose) from C57BL6/J mice (Figure 2I–J) were used. Perifusion was performed, as described previously [18]. Fc-GLP-1 (100 nM), Fc-PYY_{3-36} (1 μM), or the combination were added during the entire perifusion procedure, as shown in Figure 2I–J.

2.5. Energy expenditure

Indirect calorimetry was performed with a Columbus Instruments Comprehensive Laboratory Animal Monitoring System (CLAMS) (Columbus, OH). Cohort B consisted of 3 groups: C57BLKS/J *db/db* vehicle, C57BLKS/J *db/db* Fc-PYY_{3-36} + Fc-GLP-1 (dosed as described), and C57BLKS/J *db/db* weight matched to the drug-treated group. Animals were dosed for 16 days; on day 12, they were acclimated to the CLAMs system for 48 h. On day 14, respirometry and locomotor activity were monitored for 36 h and recorded.

2.6. Dual radiolabelled hyperinsulinaemic-euglycemic clamp and glycogen assessment

Clamp studies and associated calculations were performed as previously described [18,21]. Cohort C consisted of *db/+*, C57BLKS/J *db/db* vehicle, C57BLKS/J *db/db* Fc-PYY_{3-36} + Fc-GLP-1, and C57BLKS/J *db/db* weight-matched (WM) to the drug-treated group. Cohort D consisted of DIO C57BL6/J vehicle, DIO C57BL6/J Fc-PYY_{3-36} + Fc-GLP-1, DIO Y2RKO vehicle, and DIO Y2RKO Fc-PYY_{3-36} + Fc-GLP-1 mice (D12492, Research Diets). In both cohorts C and D, the animals were dosed with SC QAD for 1 week with a low-dose compound. The jugular vein and carotid artery catheters were placed in animals 7 days prior to the experiment. The animals were then dosed with SC QAD for an additional week with a high dose compound. On the day of the clamp study conscious, unrestrained 5 h fasted mice were simultaneously infused into the jugular vein with a constant rate of 0.1 μCi/mi [^{3}H]-glucose. After the basal period, at a variable rate of 20% dextrose to maintain target glycemia and a constant rate of human insulin was infused into the jugular vein catheter. Arterial blood samples were collected over 10 min from the arterial catheter and the glucose infusion rate was adjusted to maintain the glucose at a target concentration. For cohort C ($N \geq 6$/group), steady-state glucose was achieved at 200 mg/dL using 40 mU/min/kg (lean mass) of insulin. For cohort D ($N \geq 7$/group), steady-state glucose was achieved at 110 mg/dL using 4mU/min/kg (body weight) of insulin. At 120 min, a bolus of [^{14}C]-2-deoxy-glucose was infused to assess tissue-specific glucose uptake. At 155 min, the animals were sacrificed with pentobarbital anaesthesia and tissues collected. Total glycogen content and tracer-determined glycogen synthesis in gastrocnemius and liver were assessed, as described previously [22].

2.7. Conditioned taste aversion

One week prior to assessment, animals were single-housed with *ad libitum* access to food and one bottle of water. The position of the water bottle was switched daily to minimize the development of side preference. The animals were weighed and handled daily 3 days prior to assessment. On the day of conditioning and following 12 h of water deprivation (day 1), animals were exposed to the bottle containing highly palatable 0.1% saccharin flavored water (4 h access). Immediately after (t = 0 h), animals were IP-dosed with Fc-PYY_{3-36}, Fc-GLP-1, Fc-PYY_{3-36} + Fc-GLP-1 or cisplatin, as indicated. Seventy-two hours later, a voluntary choice between tap water and 0.1% saccharin solution was provided; both water and saccharin solution intake were measured after 24 h (between t = 72 h and 96 h).

2.8. cFOS quantitation

Animals from cohort E were IP-sham dosed for 3 days prior to termination. On the study day, animals were dosed IP with the compound as indicated, sacrificed via midazolam anaesthesia followed by isoflurane inhalation 4 h post-dose, transcardially perfused with heparinized saline (15,000 IU/L) followed by 4% paraformaldehyde for 5 min (10 mL/min) and brains removed 4 h following IP-dosing. Brains were removed, post-fixed overnight in the same fixative, transferred for 2 days to a 30% sucrose solution, cut into six series of 40 μm coronal sections on a freezing microtome, and stored until immunohistochemical processing. The cFOS immunostaining and counting of c-FOS positive cell nuclei were performed, as previously described [23]. An initial qualitative cFOS screen was performed in lean C57BL6/

J mice following the above procedure to identify regions of interest for c-FOS quantitation (data not shown).

2.9. Laser capture microdissection and RNAseq-bioinformatics

Laser capture microdissection was performed, as previously described [24,25] on brains from cohort F 4 h following IP-dosing. Briefly, snap-frozen brains were sectioned (10 μm thickness) on a Cryostat (model CM350 S, Leica Biosystems, Nussloch, Germany). Sections were collected onto polyethylene naphthalate (PEN) membrane glass slides (Thermo Fischer Scientific), fixed, crystal violet stained, and dehydrated. LCM was performed using an ArcturusXT microdissection system (Thermo Fischer Scientific, USA). A combination of the infrared capture laser and the ultraviolet cutting laser allowed isolation of 4 mm^2 tissue from each brain region per animal. RNA was isolated using the PicoPure RNA isolation kit (Thermo Fischer Scientific). RNAseq libraries were prepared with NeoPrep using the Illumina TruSeq stranded mRNA library kit for NeoPrep and sequenced (75 base pair single-end reads) on the NextSeq 500 (Illumina, San Diego, CA). Reads were aligned to the GRCm38 v89 Ensembl *Mus musculus* genome using STAR v.2.5.2a [26]. Differential gene expression (DEG) analysis was performed with the R package DEseq2 [27] and genes considered significantly regulated based on having a false discovery rate (FDR) of <0.01. A gene set analysis was conducted with the R package Piano [28] using the Stouffer method. The gene sets were defined based on the Reactome pathway database [29], and gene sets <4 genes were excluded from the analysis. The data discussed in this publication are deposited in NCBI's Gene Expression Omnibus [24,25] and are accessible through GEO Series accession number GSE160802. Gene sets were considered significantly enriched based on having a Benjamini-Hochberg corrected p-value < 0.01.

2.10. Light sheet microscopy

Twenty-four hours following IP-dosing, animals in cohort G were anesthetized with a mixture of Hypnorm (Glostrup Pharmacy, Denmark) and Dormicum (Hameln Pharma, Germany) and then perfused with heparinized (15,000 IU/L) PBS followed by 10% neutral buffered formalin (NBF). Brains were removed, post-fixed overnight at room temperature in NBF, washed in PBS and methanol dehydrated (20%, 40%, 60%, 80% and 100%, 1 h each at room temperature), and stored in 100% methanol until whole-brain immunohistochemistry, which was accomplished with a modified version of the iDISCO protocol [30]. Permeabilization was carried out at 37 °C for 3 days, blocking at 37 °C for 2 days and antibody labelling with primary anti-cFOS antibody (Cell Signaling Technology, US; cat no #2250; RRID: AB_2247211) at 37 °C for 7 days. Samples were washed and incubated with secondary antibody (donkey-anti-Rb_Cy-5, Jackson ImmunoResearch, UK; cat no #711-175-152; RRID: AB_2340607) at 37 °C for 7 days. Thereafter, brains were dehydrated in methanol/water series and cleared using 66% dichloromethane/33% methanol for 3 h, then 100% dichloromethane 2 × 15 min, and finally transferred to dibenzyl ether in closed glass vials.

Brains were imaged using a Lavision light-sheet ultramicroscope II (Miltenyi Biotec GmbH, Bergisch Gladbach, Germany)) with Zyla 4.2 P-CL10 sCMOS camera (Andor Technology, Belfast, United Kingdom), SuperK EXTREME supercontinuum white-light laser EXR-15 (NKT Photonics, Birkerod, Denmark), and MV PLAPO 2XC (Olympus, Tokyo, Japan) objective. The brain was attached to a transparent sample holder made of silicone with neutral silicone gel (ventral side up) and imaged in a chamber filled with Dibromoethane (DBE). Imspector microscope controller software (v7) was used (Miltenyi Biotec GmbH, Bergisch Gladbach, Germany). Horizontal images were acquired at 0.63x magnification (1.2 × total magnification) with an exposure time of 254 ms in a z-stack at 10 μm intervals. Horizontal focusing was captured in 9 planes with blending mode set to the center of the image to merge the individual raw images. Autofluorescence images were captured at 560 ± 20 nm (excitation) and 650 ± 25 nm (emission) wavelength (80% laser power in Imspector software, 100% NKT laser). cFOS staining was imaged at 630 ± 15 nm excitation wavelength and 680 ± 15 nm emission wavelength (100% laser power in software, 100% mechanical). Samples were scanned in a random order using identical settings.

The images were reconstructed to create a 3-D image of the entire brain and aligned to Allen's CCFv3 brain atlas [31]. To determine the difference in cFOS positive cells between light-sheet microscopy samples, a negative binomial generalized linear model was fitted to the data. Deviance residuals of the statistical model were examined to ensure alignment with assumptions of normality and homoscedasticity. Cook's distance was calculated for each data point to prevent the influence of data point on the model.

2.11. Statistics

Data normality was determined using the D'Agostino and Pearson Test. Parametric data were analysed using Student's t-test for two groups, or one or two-way ANOVA followed by Tukey's or Sidak's *post-hoc* test for >2 groups. Non-parametric data were analysed by Mann—Whitney test for 2 groups, or Kruskal—Wallis test followed by Dunn's *post-hoc* test for >2 groups. Data are presented as mean ± SE of at least 3 biological replicates (except for Figure 6F, WT, GLP-1 where only N = 2 was available due to technical error). All data were analysed using GraphPad Prism version 7.02 (GraphPad, San Diego, CA). Statistical significance was set at $p \leq 0.05$. Indirect calorimetry data were analysed by CalR [31,32] using a general linear model based on ANCOVA.

3. RESULTS

3.1. Fc-PYY_{3-36} and Fc-GLP-1 generation

Recombinant IgG1 Fc was generated with a cysteine substitution at position 442 (442C) of the CH3 domain using standard DNA recombinant technology [12] and expressed in CHO cells (Supplementary Figure 1A). The Synthetic Y2R-selective peptide was prepared by automated solid-phase synthesis with a maleimide functional group at Lysine 11 (Supplementary Figure 1B). Following reduction and oxidation, the maleimide-functionalized PYY_{3-36} was site-specifically conjugated to the Fc molecule at position 442C to yield Fc-PYY_{3-36} (Supplementary Figure 1C). Further detail is provided in the Methods section. The Fc-GLP-1R agonist was an internally generated (AstraZeneca, Gaithersburg, MD) version of Dulaglutide IgG4 Fc and was purified as per Fc-PYY_{3-36}. Stable CHO cell lines overexpressing human or mouse GLP-1R or Y2R were used for assessment of half-maximal agonist potency (EC_{50}) for inducing cAMP production (Supplementary Figs. 1D and 1E). Fc-GLP-1 showed EC_{50} 12.8 ± 2.0 pM and 41.3 ± 6.0 pM and Fc-PYY3-36 EC_{50} 1.3 ± 0.3 pM and 2.8 pM in humans and mice, respectively. Fc-PYY_{3-36} was highly specific to Y2R over Y1R, Y4R, and Y5R by at least 10,000-fold (data not shown).

3.2. Fc-PYY_{3-36} promotes diabetes remission in combination with Fc-GLP-1 in C57BLKS/J db/db mice

Eight-week-old C57BLKS/J *db/db* mice were treated with Fc-PYY_{3-36}, Fc-GLP-1, or Fc-PYY_{3-36} + Fc-GLP-1 for 4 weeks. We selected sub-maximal doses when administered as monotherapies (Fc-PYY_{3-36} 1 mg/kg and Fc-GLP-1 0.15 mg/kg) to maximise the window of

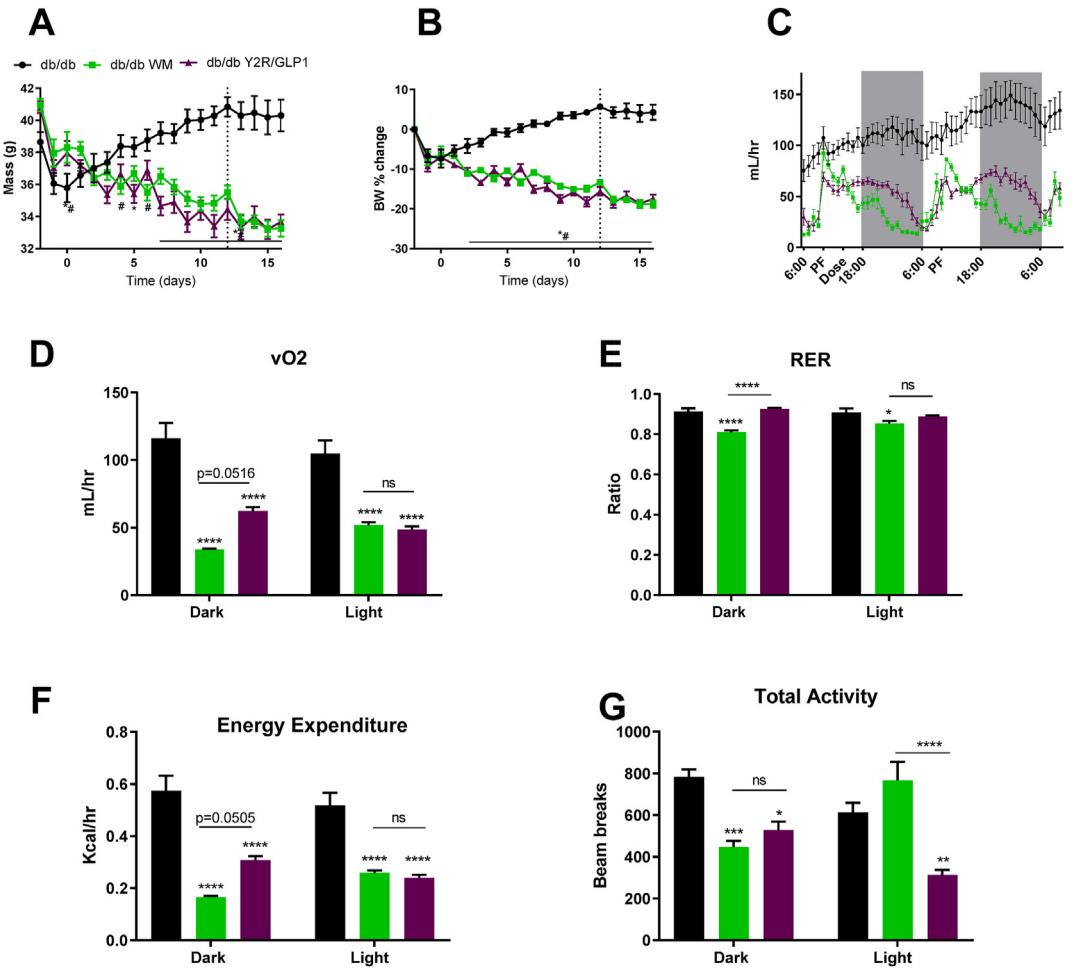

Figure 3: Effect of 2-week Fc-PYY$_{3-36}$/GLP-1 (1 mg/kg/0.15 mg/kg) treatment on energy expenditure in KS db/db mice. A) Body weight profile of study animals and B) the percentage change in body weight during the 2-week treatment period. N = 8 for all groups. The dashed line indicates the beginning of acclimation to indirect calorimetry cages. Indirect calorimetry recording began on day 14. *p ≤ 0.05 db/db vs db/db Fc-PYY$_{3-36}$/GLP-1, #p ≤ 0.05 db/db vs db/db WM. C) real-time vO2 and D) vO2 from 48-hr light (24 h) and dark (24 h) periods. E) RER, F) regression plot of energy expenditure as a function of body weight and G) total activity from 48-hr light (24 h) and dark (24 h) periods. N = 8 for all groups. **p ≤ 0.01 vs Vehicle, ***p ≤ 0.001 vs Vehicle, ****p ≤ 0.0001 vs Vehicle. Asterisks above a line indicate significance between groups.

opportunity to examine the synergistic potential of combination treatment. Though unchanged between monotherapy and vehicle-treated animals, body weights were significantly reduced by 7% in Fc-PYY$_{3-36}$ + Fc-GLP-1 versus vehicle-treated mice (Figure 1A, B). Vehicle-treated animals displayed an ∼4-point increase in %HbA1c which was significantly mitigated by both monotherapy treatments, while Fc-PYY$_{3-36}$ + Fc-GLP-1 treatment led to a 0.7-point reduction in %HbA1c over the study period, leading to an ∼5-point decrease in %HbA1c relative to the vehicle control (Figure 1C). At week 3 of treatment, glucose tolerance was unchanged with either monotherapy treatment but was significantly improved in the Fc-PYY$_{3-36}$ + Fc-GLP-1 combination group (Figure 1D) amounting to a 33% reduction in glucose AUC (Figure 1E). Fasting plasma blood glucose was not different after Fc-PYY$_{3-36}$ or Fc-GLP-1 treatment versus vehicle (control); however, the combination of Fc-PYY$_{3-36}$ + Fc-GLP-1 significantly reduced plasma glucose by ∼66% (Figure 1F). The decreased fasting plasma glucose levels were paralleled by corresponding increases in fasting insulin levels, for both Fc-GLP-1 and Fc-PYY$_{3-36}$ + Fc-GLP-1 (Figure 1G). Pancreatic insulin content was unchanged at termination by monotherapy treatment but was strongly increased by Fc-PYY$_{3-36}$ + Fc-GLP-1 combination treatment by over 8-fold (Figure 1H), implicating possible enhanced β-cell function and/or mass as a contributor to the synergistic improvement in metabolic homeostasis induced by peptide co-administration.

Hence, primary pancreatic islets were isolated from vehicle and Fc-PYY$_{3-36}$ + Fc-GLP-1 treated animals. Islets were subjected to dynamic perifusion with 2.8 mM glucose (basal) for 40 min followed by 16.7 mM glucose (stimulatory) for 50 min (Figure 2A). Islets from combination-treated animals displayed >6-fold increase in first-phase insulin secretion, and >7-fold increase in second-phase insulin secretion, suggesting a marked recovery in β-cell insulin secretory capacity (Figure 2B). Expressions of key genes related to β-cell function, including *Ins1, Ins2, Gck, Slca2a, Pdx1,* and *Mafa* were all significantly increased in islets from combination-treated versus vehicle-treated mice (Figure 2C). Electron micrograph analysis of β-cells from vehicle-treated mice indicates a significant decrease of the mature insulin secretory granule population and expansion of the rough endoplasmic reticulum/Golgi apparatus compartments (Figure 2D), while Fc-PYY$_{3-36}$ + Fc-GLP-1-treated animals exhibited recovery of insulin secretory granule numbers and normalized morphology of other organelles (Figure 2E). This is consistent with previous studies of physiological and pharmacological restoration of β-cell function

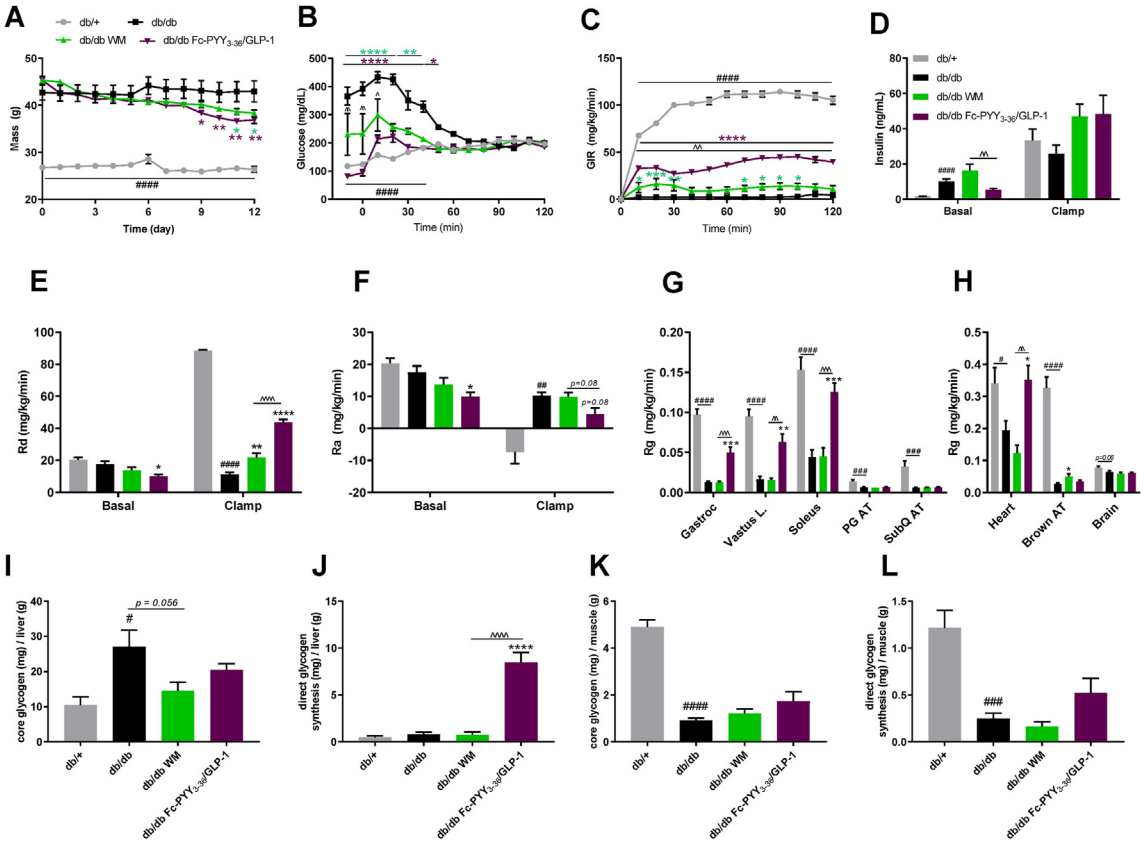

Figure 4: Hyperinsulinemic/euglycemic clamp following 2-week Fc-PYY$_{3-36}$/GLP-1 (1 mg/kg/0.15 mg/kg) treatment in KS *db/db* mice. A) Body weight profile of study animals. B) Plasma glucose levels during the clamp. C) Glucose infusion rate required to maintain euglycemia (200 mg/dL) during the clamp. $^{*}p \leq 0.05$ db/db vs db/db Fc-PYY$_{3-36}$/GLP-1, $\#p \leq 0.05$ db/db vs db/db WM. D) Basal and insulin-stimulated plasma insulin levels. E) Basal and insulin-stimulated peripheral glucose disposal (Rd). F) Basal and insulin-stimulated endogenous glucose production (Rg). G) Tissue-specific insulin-stimulated glucose disposal for gastrocnemius, vastus lateralis, soleus, perigonadal and subcutaneous adipose tissue and H) heart, brown adipose tissue, and brain. I) Core liver glycogen. J) Direct liver glycogen synthesis. K) Core muscle glycogen. L) Direct muscle glycogen synthesis. N = 5–10. $\#p \leq 0.05$, $\#\#p \leq 0.01$, $\#\#\#p \leq 0.001$, $\#\#\#\#p \leq 0.0001$ vs *db/+* . $^{*}p \leq 0.05$, $^{**}p \leq 0.01$, $^{***}p \leq 0.001$, $^{****}p \leq 0.0001$ vs *db/db* vehicle. $\hat{}p \leq 0.05$, $\hat{}p \leq 0.01$, $\hat{}p \leq 0.001$, $\hat{}p \leq 0.0001$, Fc-PYY$_{3-36}$/GLP-1 vs WM. For (A–C) Sidak's multiple comparisons test *db/+* vs *db/db* to determine the effect of genotype. One-way ANOVA with repeated measured followed by Tukey's multiple comparisons test with *db/+* excluded to determine the effect of treatment. For (D–L) unpaired t-test *db/+* vs *db/db* to determine the effect of genotype. One-way ANOVA followed by Tukey's multiple comparisons test with *db/+* excluded to determine the effect of treatment.

[17,18,20]. Image quantification revealed that the number of mature insulin secretory granules per β-cell cytoplasmic area was increased by over 5-fold in Fc-PYY$_{3-36}$ + Fc-GLP-1-treated animals (Figure 2F), in parallel with the enhancement in total pancreatic insulin content. The population of immature insulin secretory granules was also reduced by Fc-PYY$_{3-36}$ + Fc-GLP-1, supporting improved functional capacity in these treated islet β-cells (Figure 2G). Additional representative electron micrographs are also shown (Supplementary Figure 2), as further evidence of the adaptive plasticity of pancreatic β-cells and restoration of the mature insulin secretory granule store by Fc-PYY$_{3-36}$ + Fc-GLP-1-treatment. Morphometric analysis of insulin and glucagon immunohistochemical co-stained sections indicated unaltered pancreatic α-cell mass but an apparent increase in pancreatic β-cell mass, as assessed by insulin-positive staining, in Fc-PYY$_{3-36}$ + Fc-GLP-1-treated animals (Figure 2H). Representative images of pancreatic islets (Supplementary Figure 3) indicate little change in β-cell proliferation as previously observed (Boland et al., 2019b), and more intensive insulin and MafA staining complementary to increased pancreatic islet insulin content (Figures 2H and 2D-G) and *MafA* gene expression (Figure 2C). To exclude a direct effect of Fc-PYY$_{3-36}$ on islets, overnight cultured primary islets from naïve C57BL6/J mice underwent perifusion at basal (2.8 mM) and stimulatory (16.7 mM) glucose in the presence of Fc-GLP-1 (100 nM), Fc-PYY$_{3-36}$ (1 μM) or the combination (Figure 2I). Fc-GLP-1 potentiated glucose-stimulated insulin secretion; however, Fc-PYY$_{3-36}$ had no effect alone and did not enhance the Fc-GLP-1 response (Figure 2J).

3.3. Fc-PYY$_{3-36}$ + Fc-GLP-1 does not affect RER but reduces total activity and VO_2

To identify physiological changes that could account for the weight loss and improvements in glucose homeostasis induced by Fc-PYY$_{3-36}$ + Fc-GLP-1 combination treatment, indirect calorimetry assessment of C57BLKS/J *db/db* mice treated with vehicle, Fc-PYY$_{3-36}$ + Fc-GLP-1, or vehicle and weight-matched (WM) to Fc-PYY$_{3-36}$ + Fc-GLP-1-treated mice via food restriction was conducted. Vehicle-treated mice gained weight throughout the study period while both Fc-PYY$_{3-36}$ + Fc-GLP-treated and WM controls lost approximately 15% of body weight at the time of indirect calorimetry (Figure 3A, B). VO_2 was reduced in Fc-PYY$_{3-36}$ + Fc-GLP-1-treated and WM animals relative to the controls during both light and dark phases, but this effect was more pronounced during the dark phase in WM mice (Figure 3C, D). The respiratory exchange ratio (RER) was reduced in WM animals but

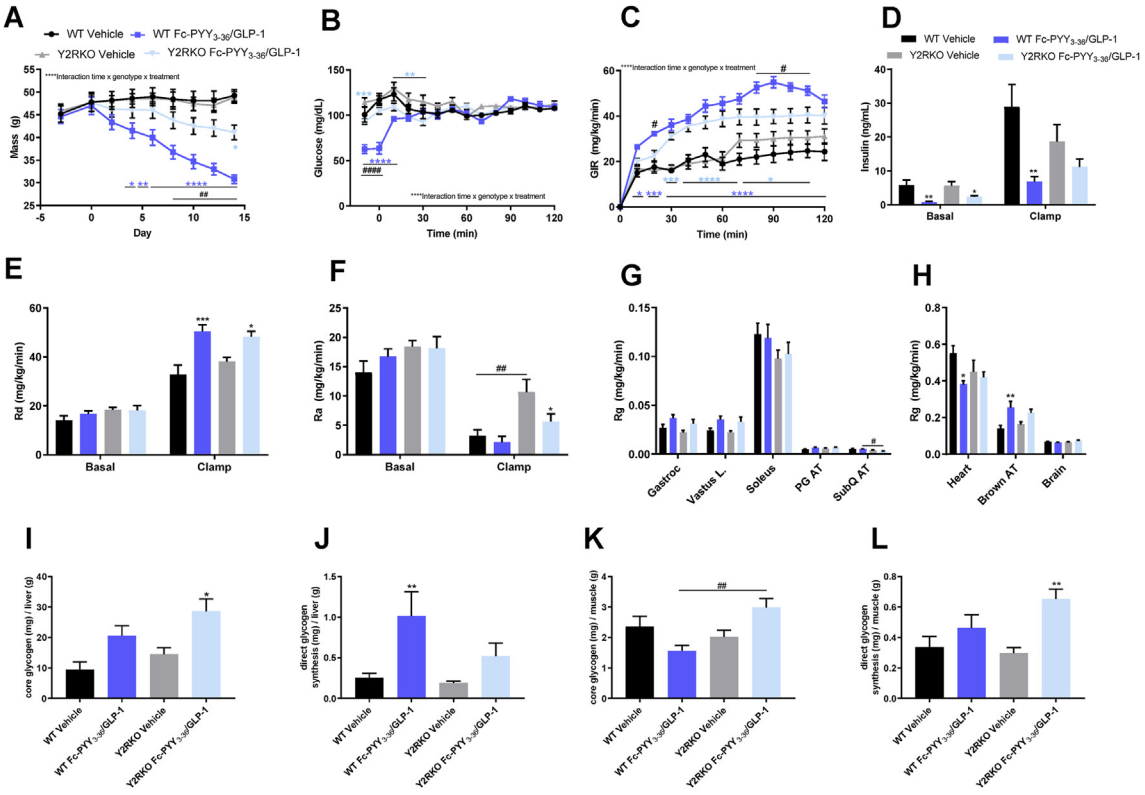

Figure 5: Hyperinsulinaemic/euglycemic clamp following 2-week Fc-PYY$_{3-36}$/GLP-1 (1 mg/kg/0.15 mg/kg) treatment in DIO WT and Y2RKO mice. A) Body weight profile of study animals. B) Plasma glucose levels during the clamp. C) Glucose infusion rate required to maintain euglycemia (110 mg/dL) during the clamp. $*p \leq 0.05$ WT Vehicle vs WT Fc-PYY$_{3-36}$/GLP-1, $\#p \leq 0.05$ WT Vehicle vs Y2RKO Fc-PYY$_{3-36}$/GLP-1. D) Basal and insulin-stimulated plasma insulin levels. E) Basal and insulin-stimulated peripheral glucose disposal (Rd). F) Basal and insulin-stimulated endogenous glucose production (Rg). G) Tissue-specific insulin-stimulated glucose disposal for gastrocnemius, vastus lateralis, soleus, perigonadal and subcutaneous adipose tissue and H) heart, brown adipose tissue and brain. I) Core liver glycogen. J) Direct liver glycogen synthesis. K) Core muscle glycogen. L) Direct muscle glycogen synthesis. N = 5–10. $*p \leq 0.05$, $**p \leq 0.01$, $***p \leq 0.001$, $****p \leq 0.0001$, vs vehicle within genotype. $\#p \leq 0.05$, $\#\#p \leq 0.01$, $\#\#\#\#p \leq 0.0001$ WT vs Y2RKO within treatment. For (A–C) two-way ANOVA with repeated measures followed by Tukey's multiple comparisons test. For (D–L) two-way ANOVA followed by Sidak's multiple comparisons test.

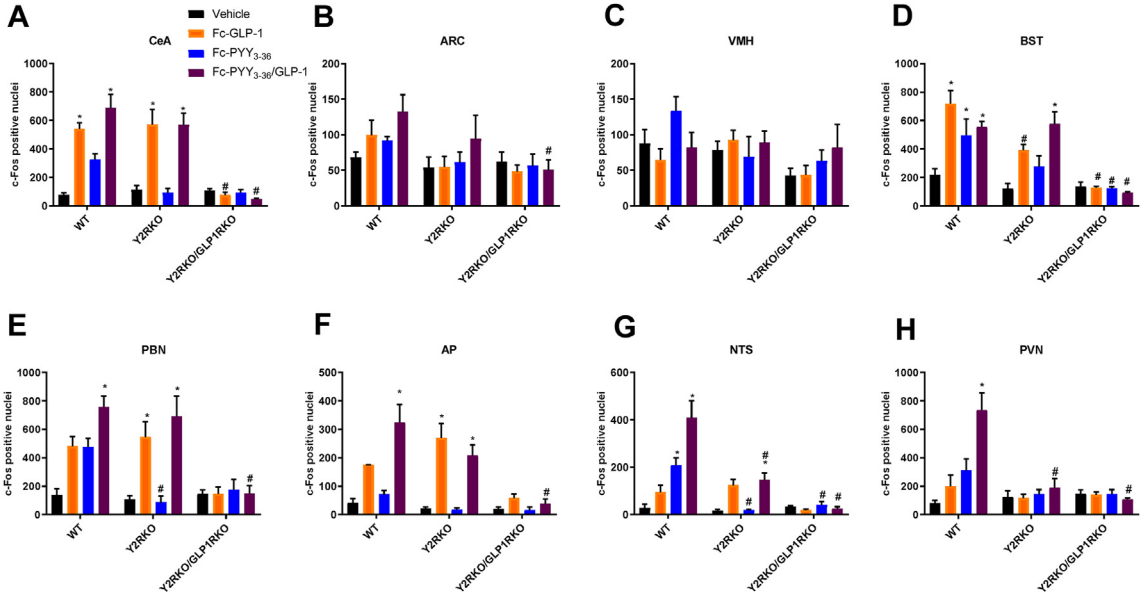

Figure 6: Quantitation of cFOS-positive cells in selected brain regions of lean WT, Y2RKO, and Y2RKO/GLP1RKO mice 4 h following IP-administered Fc-PYY$_{3-36}$ (1.0 mg/kg), Fc-GLP-1 (0.15 mg/kg) or Fc-PYY$_{3-36}$/GLP-1 (1.0 mg/kg/0.15 mg/kg) combination. The average stained number of cFOS positive cells in the A) central nucleus of the amygdala (CeA), B) arcuate nucleus (ARC), C) ventromedial hypothalamic nucleus (VMH), D) bed of the stria terminalus (BST), E) parabrachial nucleus (PBN), F) area postrema (AP), G) nucleus of the solitary tract (NTS), and H) paraventricular hypothalamic nucleus (PVN) are shown. $*p \leq 0.05$ vs Vehicle, same genotype $\#p \leq$ vs WT, same treatment. N = 2–5.

increased by Fc-PYY$_{3-36}$ + Fc-GLP-1 treatment during the dark phase (Figure 3E). Energy expenditure was reduced in both Fc-PYY$_{3-36}$ + Fc-GLP-1-treated and WM animals compared to db/db but energy expenditure was increased in Fc-PYY$_{3-36}$ + Fc-GLP-1-treated animals compared to WM animals (Figure 3F). Total physical activity was decreased during both light and dark phases in Fc-PYY$_{3-36}$ + Fc-GLP-1-treated animals but only during the dark phase in WM controls (Figure 3G). Common side effects of GLP-1 and Fc-PYY$_{3-36}$ agonism include nausea [48] and emesis [33], respectively. Therefore, we assessed the potential for an aversive response to Fc-GLP-1, Fc-PYY$_{3-36}$ and the combination in naïve lean C57BL6/J mice using a conditioned saccharin preference test. All animals demonstrated similar saccharin intake prior to dosing (Supplementary Figure 4A), and all compounds induced weight loss following acute administration (Supplementary Figs. 4B and 4C). Over a 24-h period following compound administration (72–96 h post-dose), total fluid intake was significantly reduced in groups receiving cisplatin (positive control) and Fc-GLP-1 (Supplementary Figure 4D). Water intake was significantly increased in all treatment groups (Supplementary Figure 4E). Saccharin intake, saccharin preference, and the consumed saccharin to water ratio were all significantly reduced by cisplatin and Fc-PYY$_{3-36}$ + Fc-GLP-1 (Supplementary Figs. 4F, 4G, 4H). These data indicate that the combination of Fc-PYY$_{3-36}$ + Fc-GLP-1 induces a greater degree of aversive behaviour than either monotherapy.

3.4. Fc-PYY$_{3-36}$ + Fc-GLP-1 improves insulin sensitivity and hepatic glycogen synthesis independent of weight loss in C57BLKS/J db/db mice

To explore weight-independent mechanisms of Fc-PYY$_{3-36}$ + Fc-GLP-1 on insulin action, a hyperinsulinaemic-euglycemic clamp in severely insulin-resistant obese/diabetic C57BLKS/J *db/db* mice treated with vehicle or Fc-PYY$_{3-36}$ + Fc-GLP-1 for 2 weeks was performed. Control groups consisted of C57BLKS/J *db/db* mice weight-matched (WM) to the Fc-PYY$_{3-36}$ + Fc-GLP-1 group and lean C57BLKS/J *db/+* mice. Db/+ mice were much lighter than their db/db counterparts with Fc-PYY$_{3-36}$ + Fc-GLP-1 administration inducing a 14% body weight reduction over the 2-week period, and WM-controls exhibited similar reductions (Figure 4A, Supplementary Figure 5A). In consideration of divergent starting blood glucose concentrations (121 mg/dL in C57BLKS/J *db/+* mice versus 404 mg/dL in C57BLKS/J *db/db* mice in the basal period t = −10 to 0 min; Figure 4B; Supplementary Figure 5B), glucose levels were clamped at 200 mg/dL with glucose stabilized between groups by 60 min of clamp (Figure 4B). Fc-PYY$_{3-36}$ + Fc-GLP-1 led to ∼20-fold increase in the glucose-infusion rate (GIR) versus vehicle db/db animals, which was significantly higher than WM controls, indicating weight loss-independent effects of Fc-PYY$_{3-36}$ + Fc-GLP-1 on enhanced insulin sensitivity (Figure 4C), although the possibility of an altered weight-dependence to insulin sensitivity cannot be ruled out. Basal insulin levels were elevated in db/db mice compared to db/+ and reduced by Fc-PYY$_{3-36}$ + Fc-GLP-1-treated animals compared with WM controls (Figure 4D). During the insulin-infusion (i.e., clamp) period insulin levels were not different between groups (Figure 4D). Using tracer approaches, the impact on hepatic and extrahepatic glucose metabolism was assessed. Basal whole-body glucose disposal (Rd; Figure 4E) and hepatic glucose production (Ra; Figure 4F) were both significantly reduced by Fc-PYY$_{3-36}$ + Fc-GLP-1 treatment compared with vehicle and is reflective of reduced basal whole-body glucose turnover contributing to the decrease in basal glucose levels (Figure 4B and Supplementary Figure 5B). Under insulin-stimulated conditions, Rd was strongly increased in db/+ mice compared to db/db vehicle. Both WM and Fc-PYY$_{3-36}$ + Fc-GLP-1 groups increase Rd compared to vehicle-treated animals and Fc-PYY$_{3-36}$ + Fc-GLP-1 was further enhance compared with WM consistent with the observed increase in glucose infusion rate (Figure 4E). Fc-PYY$_{3-36}$ + Fc-GLP-1 treatment shifted the relationship observed between Rd and circulating insulin levels to the left (i.e. increased insulin sensitivity) toward that seen in lean controls but was not observed in the WM group (Supplementary Figure 5C). During the clamp period, insulin trended to suppress endogenous glucose production (EGP) more so with Fc-PYY$_{3-36}$ + Fc-GLP-1 treatment as compared with WM and vehicle-treated animals ($p=0.08$; Figure 4F) despite similar insulin levels (Supplementary Figure 5D). To determine the site for the enhancement in peripheral glucose disposal we assessed tissue-specific glucose uptake (Rg). Tissue-specific glucose uptake was enhanced in all db/+ tissues evaluated compared with db/db vehicle (Figure 4G,H). Fc-PYY$_{3-36}$ + Fc-GLP-1 treatment enhanced skeletal muscle (gastrocnemius, vastus, and soleus) and cardiac glucose uptake to levels compared with *db/db* vehicle and WM mice (Figures 4G and 5H). WM mice demonstrated increased uptake of brown adipose tissue glucose compared with vehicle only (Figure 4H). As the clamps were performed at mild hyperglycaemia (200 mg/dl) that could augment hepatic glycogen synthesis, we assessed the core glycogen stores as well as tracer-determined (direct) glycogen synthesis. Core hepatic glycogen was increased in *db/db* vehicle compared to lean *db/+* mice, which is consistent with their basal hyperglycaemia and trended towards being reduced by WM ($p = 0.056$; Figure 4I). Fc-PYY$_{3-36}$ + Fc-GLP-1 dramatically increased insulin-stimulated hepatic glycogen synthesis (Figure 4J). In contrast with the liver, core, and insulin-stimulated skeletal muscle glycogen synthesis was significantly reduced in *db/db* mice compared with *db/+* and were not increased by Fc-PYY$_{3-36}$ + Fc-GLP-1 combination or WM (Figure 4K, 4 L).

3.5. Fc-PYY$_{3-36}$ + Fc-GLP-1 enhancement of hepatic glycogen synthesis, but not skeletal muscle glucose uptake, requires Y2R agonism in diet-induced obese (DIO) mice

To better characterize the contribution of the GLP-1R to Fc-PYY$_{3-36}$ + Fc-GLP-1 pharmacology, hyperinsulinaemic-euglycemic clamps were performed in DIO WT and Y2RKO mice to examine the impact of Fc-PYY$_{3-36}$ + Fc-GLP-1 dual agonism on insulin action. Body weight loss and reduced fasting glucose induced by Fc-PYY$_{3-36}$ + Fc-GLP-1 dual agonism were blunted in Y2RKO versus WT mice (14% vs 32%, body weight, respectively) (Figure 5A, Supplementary Figure 6A). Fasting glucose was reduced by Fc-PYY$_{3-36}$ + Fc-GLP-1 in both WT and Y2RKO with a significantly greater magnitude in WT mice (Figure 5B and Supplementary Figure 6B). Glucose was clamped at 110 mg/dL and was stabilized between groups by 30 min of insulin infusion (Figure 5B). GIR was significantly increased by Fc-PYY$_{3-36}$ + Fc-GLP-1 dual agonism in both genotypes compared with their respective vehicle groups and was further increased in WT Fc-PYY$_{3-36}$ + Fc-GLP-1 vs. Y2RKO Fc-PYY$_{3-36}$ + Fc-GLP-1 mice from 80 to 110 min (Figure 5C). Basal insulin levels were significantly decreased by Fc-PYY$_{3-36}$ + Fc-GLP-1 dual agonism WT and Y2RKO mice compared with their respective vehicle controls (Figure 5D). Under clamp conditions, WT mice administered the Fc-PYY$_{3-36}$ + Fc-GLP-1 combination demonstrated significantly reduced insulin levels compared to the WT vehicle (Figure 5D), despite the equal concentration of insulin infusion. One limitation of this experiment is the absence of C-peptide analysis to better elucidate the contribution of endogenous insulin secretion vs. insulin clearance in this effect. Basal whole-body glucose disposal was not different between groups but was significantly and similarly increased in both WT and Y2RKO mice

administered Fc-PYY$_{3-36}$ + Fc-GLP-1 combination (Figure 5E), with a clear relationship between circulating insulin levels and whole-body glucose disposal observed (Supplementary Figure 6C). These data indicate that the presence of Y2R signalling played a minor role in the insulin-sensitizing effects of Fc-PYY$_{3-36}$ + Fc-GLP-1 dual agonism and GLP-1R signalling was sufficient to maximize the insulin-sensitizing effect. Basal hepatic glucose production (Ra) was not different between groups (Figure 5F). During the clamp, hepatic glucose production was equally suppressed in WT mice regardless of treatment (Figure 5F). However, Ra was elevated in the Y2RKO vehicle compared with the WT vehicle; this was significantly reduced by Fc-PYY$_{3-36}$ + Fc-GLP-1 treatment in Y2RKO mice (Figure 5F). The suppression of hepatic glucose production during clamp conditions in Fc-PYY$_{3-36}$ + Fc-GLP-1 treated mice showed an improved relationship with circulating insulin levels by a shift of the curve to the left and steeper slope suggesting improved hepatic insulin sensitivity (Supplementary Figure 6D). Similar to the findings in C57BLKS/J *db/db* mice, there was a trend for a treatment effect of Fc-PYY$_{3-36}$ + Fc-GLP-1 dual agonism to increase skeletal muscle (gastric and vastus) glucose uptake, albeit not significant (Figure 5G). However, Fc-PYY$_{3-36}$ + Fc-GLP-1 administration significantly increased brown adipose tissue and decrease cardiac glucose uptake in WT mice (Figure 5H). Core hepatic glycogen levels were significantly increased in Y2RKO mice administered Fc-PYY$_{3-36}$ + Fc-GLP-1 compared with Y2RKO vehicle (Figure 5I). Insulin-stimulated hepatic glycogen synthesis was significantly increased in WT mice administered Fc-PYY$_{3-36}$ + Fc-GLP-1 compared with WT vehicle (Figure 5J). Core skeletal muscle glycogen levels were remarkably increased in Y2RKO versus WT mice when both were administered Fc-PYY$_{3-36}$ + Fc-GLP-1 (Figure 5I), and skeletal muscle insulin-stimulated glycogen synthesis was significantly increased in Y2RKO mice administered Fc-PYY$_{3-36}$ + Fc-GLP-1 compared with Y2RKO vehicle (Figure 5J).

3.6. Fc-PYY$_{3-36}$ + Fc-GLP-1 activate discrete hypothalamic and brainstem nuclei following acute administration

This physiological data indicate that a putative mechanism for the metabolic effects of a Fc-PYY$_{3-36}$ + Fc-GLP-1 combination could be increased insulin sensitivity in the liver and perhaps skeletal muscle. As neither *Glp1r* nor *Npy2r* are expressed in these tissues (GEO datasets, NCBI), we excluded direct action in these tissues as a mechanism for the efficacy of Fc-PYY$_{3-36}$ + Fc-GLP-1 treatment. The role of the central nervous system (CNS), particularly the hypothalamus, in regulating appetite, body weight, energy expenditure, and metabolic homeostasis may influence insulin sensitivity. As such, a qualitative screen of cFOS activation (as a surrogate marker of neuronal activation) throughout the brain of lean C57BL6/J mice 4 h following a single administration of Fc-GLP-1, Fc-PYY$_{3-36}$, or Fc-PYY$_{3-36}$ + Fc-GLP-1 was conducted. Furthermore, to better define the contribution of *Npy2r* and *Glp1r* to the activation of cFOS under the same treatments, we acutely dosed naïve lean Y2RKO knockout, and Y2RKO/GLP-1RKO double knockout mice [16] and performed the same analysis (Figure 6 and Supplementary Figure 7). cFOS expression in the central nucleus of the amygdala (CeA) was strongly induced by Fc-GLP-1, and loss of Y2R did not affect the magnitude of the cFOS response in either Fc-GLP-1 or Fc-PYY$_{3-36}$ + Fc-GLP-1 administered animals, indicating that the effect was solely dependent on the GLP-1R (Figure 6A). Neither the arcuate nucleus (ARC) nor the ventromedial hypothalamic nucleus (VMH) were activated by Fc-GLP-1 or Fc-PYY$_{3-36}$ + Fc-GLP-1, which may be a consequence of assessing cFOS 4 h after administration rather than an earlier timepoint (Figure 6B, C). The bed of the stria terminalis (BST) was significantly activated by both Fc-GLP-1 and Fc-PYY$_{3-36}$, but no additive effect of the combination was observed (Figure 6D). Loss of Y2R blunted both Fc-GLP-1 and Fc-PYY$_{3-36}$-monotherapy mediated activation, but the combination maintained a similar response as that observed in WT animals (Figure 6D). The parabrachial nucleus (PBN) tended to be activated by monotherapy administration of either Fc-PYY$_{3-36}$ or Fc-GLP-1, but was significantly increased by Fc-PYY$_{3-36}$ + Fc-GLP-1 ($p < 0.0001$). Loss of Y2R did not affect the magnitude of the cFOS response of Fc-GLP-1, alone or in combination with Fc-PYY$_{3-36}$, indicating exclusive GLP-1R mediation of the observed effect (Figure 6E). While Fc-PYY$_{3-36}$ alone had no effect in the area postrema (AP), some interaction was observed when administered in combination with Fc-GLP-1 (Figure 6F). Both the nuclei of the solitary tract (NTS) and the paraventricular nucleus of the hypothalamus (PVN) demonstrated increased cFOS activation following either Fc-PYY$_{3-36}$ or Fc-GLP-1 monotherapy administration, although this only achieved significance in the NTS following Fc-PYY$_{3-36}$ monotherapy administration (Figure 6G, H). However, marked synergistic cFOS activation following Fc-PYY$_{3-36}$ + Fc-GLP-1 administration, which was strongly blunted in animals lacking Y2R, was evident in both the NTS and PVN, implicating both the hindbrain and the hypothalamus as putative mediators of the early synergistic action of Fc-PYY$_{3-36}$ + Fc-GLP-1 (Figure 6G, H).

To further characterize the early transcriptomic changes induced by Fc-PYY$_{3-36}$ + Fc-GLP-1 co-agonism, laser capture microdissection was utilized to isolate the NTS, ARC, and PVN from lean C57BL6/J mice 4 h following compound co-administration and performed RNA sequencing. PCA revealed segregation by brain region but not co-agonist administration (Supplementary Figure 8A). Fc-PYY$_{3-36}$ + Fc-GLP-1 co-administration led predominantly to down-regulation of gene expression in all regions, with the PVN showing the most abundant number of differentially up- and down-regulated genes versus the ARC and NTS (Supplementary Figure 8B). The Reactome database analysis revealed significant regulation by Fc-PYY$_{3-36}$ + Fc-GLP-1 combination in the NTS of several potential metabolic and signalling pathways (Supplementary Figure 8C), but the ARC did not demonstrate any significantly regulated gene sets at the cut-off of $p < 0.01$. From this analysis, we provide the relative gene expression levels (z-scores) of significantly up- or down-regulated genes (Supplementary Figure 8D). Numerous genes related to energy metabolism and growth, including *Fox01, Btg2, Socs3,* and *Sdc4,* were found to be highly regulated in the PVN, as well as genes associated with neuronal plasticity and development, including *Sdc4, Hs3st1,* and *Hs3st2*.

As the early (4 h) synergistic activation of appetite-regulating neurons in the hypothalamus and hindbrain likely initiates the cascade of pro-metabolic effects exerted by Fc-PYY$_{3-36}$ + Fc-GLP-1 combination, we next examined global cFOS reactivity 24 h following acute monotherapy and co-agonist administration to better indicate downstream neuronal activity and to identify a putative functional link between neuronal activation and physiological effects of Fc-PYY$_{3-36}$ + Fc-GLP-1 co-administration. Fluorescent light-sheet microscopy analysis of whole-brains from lean C57BL6/J mice 24 h following Fc-PYY$_{3-36}$, Fc-GLP-1, or Fc-PYY$_{3-36}$ + Fc-GLP-1 combination revealed that most of the hypothalamic and hindbrain areas of the brain that were significantly activated at 4 h by co-agonist administration were largely unaffected at 24 h. Both the CeA and PBN showed significantly increased cFOS reactivity following Fc-PYY$_{3-36}$ + Fc-GLP-1 co-administration, although the magnitude of activation was markedly reduced versus that observed at 4 h (Figure 7A, E). The ARC was not significantly activated, although a clear trend towards increased cFOS reactivity due to Fc-GLP-1 was present (Figure 7B). Similarly, the BST, AP, and PVN were not significantly activated by a Fc-PYY$_{3-36}$ + Fc-GLP-1

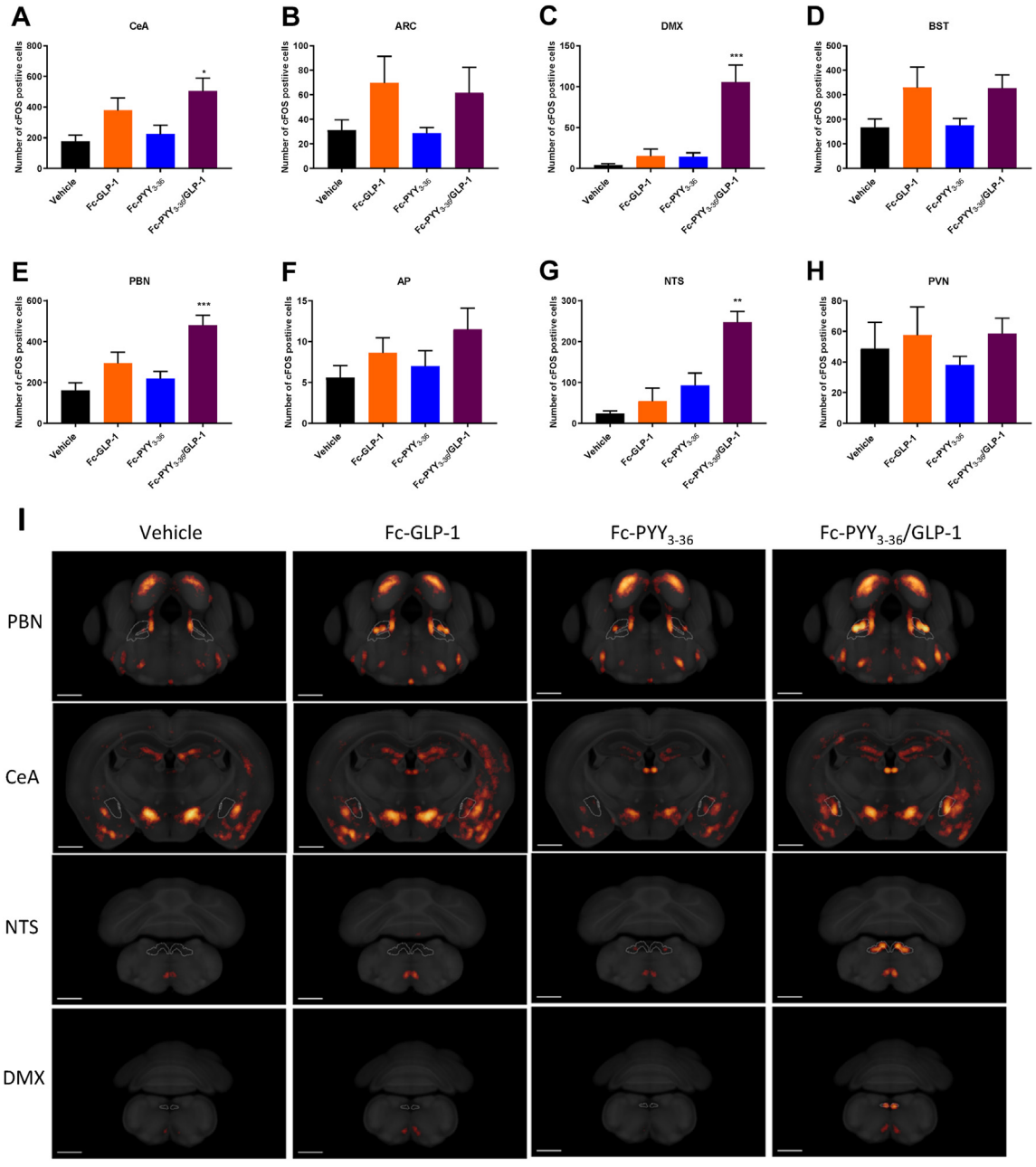

Figure 7: Whole-brain cFOS quantitation of selected regions of brain 24 h following IP-administered Fc-PYY$_{3-36}$ (1.0 mg/kg), Fc-GLP-1 (0.5 mg/kg) or Fc-PYY$_{3-36}$/GLP-1 (1.0 mg/kg/0.5 mg/kg) combination in lean C57BL6J mice. The total number of cFOS positive cells in the A) arcuate nucleus (ARC), B) paraventricular nucleus (PVN), C) area postrema (AP), D) bed of the stria terminalus (BST), E) central nucleus of the amygdala (CeA), F) parabrachial nucleus (PBN), G) nucleus of the solitary tract (NTS), H) dorsal motor nucleus of the vagal nerve (DMX) as assessed by light-sheet fluorescent microscopy. I) Selected coronal sections from group averaged brains (scale bar = 1 mm). Brain regions delineated by a dashed outline.

combination, although a trend towards activation by Fc-GLP-1 in the AP and BST was observed (Figure 7D,F, 7H). The dorsal motor nucleus of the vagus nerve (DMX), which resides in the medulla and is an area of the brain that was seemingly unaffected, and therefore not quantified at 4 h, was the most markedly activated region 24 h post Fc-PYY$_{3-36}$ + Fc-GLP-1 co-agonist administration (Figure 7C). The clear synergistic activation of cFOS in the NTS by Fc-PYY$_{3-36}$ + Fc-GLP-1 combination observed at 4 h remained present at 24 h (Figure 7G). Representative coronal sections from selected brain areas are shown in Figure 7I. A list of the top 15 most activated brain regions by Fc-PYY$_{3-36}$ + Fc-GLP-1 co-administration in Supplementary Table 1. Collectively, these data indicate that at least in part, the synergistic action of Fc-PYY$_{3-36}$ + Fc-GLP-1 combination is mediated by acute activation of neuronal circuitry in the CeA, PBN, and NTS that is sustained up to 24 h post-administration specifically in the NTS region of the brain stem.

4. DISCUSSION

The growing global burden of obesity and its associated comorbidities, including type 2 diabetes (T2D), has necessitated the development of multifaceted therapeutics that not only address glucose control and weight loss but also significantly delay the onset of comorbidities such as cardiovascular and renal complications, as well as reduce the risk of several cancers [34—37]. The observation that GLP-1 and PYY_{3-36} peptides, co-secreted from intestinal L-cells [38—40], are acutely increased after bariatric-surgery and may act as effectors for reversal of type 2 diabetes independent of weight loss has led to numerous investigations into the utility of GLP-1/PYY_{3-36} combination therapy in obesity and diabetes [34,35]. Indeed, several PYY_{3-36} analogs and Y2 receptor agonists are currently being developed in combination with GLP-1 analogs for this indication [33,41,42], and a therapeutic combination of GLP-1 and PYY_{3-36} has demonstrated synergistic effects on energy intake in humans [11,43,44]. However, although clear effects on energy intake and weight loss have also been observed preclinically in rodents, the mechanism(s) underlying the efficacy of combining these gut-peptides has remained poorly understood [38—40].

Here, we demonstrate impressive synergistic pharmacological effects of long-acting GLP-1 and PYY_{3-36} on body weight loss, glucose control, restoration of β-cell function and remission of diabetes in the C57BLKS/J *db/db* mouse model of profound obesity with severe diabetes [18,20,45]. Moreover, in a moderate model of obesity/diabetes, the DIO C57BL6/J mice, hyperinsulinemic-euglycemic clamp studies revealed Fc-PYY_{3-36} + Fc-GLP-1 combination treatment improved insulin sensitivity as indicated by reduced insulin levels during the clamp with no significant change in hepatic glucose production yet increased glucose disposal in the liver, BAT and potentially skeletal muscle. The insulin sensitization could not be explained by the accompanying weight loss alone. This Fc-PYY_{3-36} + Fc-GLP-1 combination led to activation of distinct brain regions related to appetite and energy homeostasis compared to monotherapies, underlining that a coordinated central and peripheral action is likely required to be an effective approach for the treatment of obesity-linked T2D.

Considering quite inadequate β-cell adaptive compensation underlying severe type 2 diabetes in C57BLKS/J *db/db* mice [18,20,45], the observations of normalized glycemia together with a marked improvement in endogenous β-cell function with Fc-PYY_{3-36} + Fc-GLP-1 combination treatment versus Fc-GLP-1 monotherapy were noteworthy. There was an apparent increase in β-cell mass as well as replenishment of insulin secretory granule insulin stores in parallel with an increase in total pancreatic insulin content. This restoration of endogenous insulin secretory capacity, in turn, led to a more effective biphasic glucose-stimulated insulin secretion. A cautionary note should be made about the measure of β-cell mass, since insulin itself was used as a marker for this analysis. Indeed, we report a >5-fold increase of insulin secretory granules with Fc-PYY_{3-36} + Fc-GLP-1 treatment (Figure 2D—F),. Therefore an apparent expansion of β-cell mass could actually reflect β-cell functional adaptation in restoration of insulin secretory stores rather than any increase in β-cell numbers *per se* as we have previously indicated [16,18,20,45]. There was no direct effect of Fc-PYY_{3-36} on insulin secretion *ex vivo*, thus *in vivo* improvements in β-cell function by Fc-PYY_{3-36} in synergy with Fc-GLP-1 are likely driven by physiological alterations rather than direct action of PYY_{3-36} on the β-cell itself. Consideration in these experiments is the age of the animal since our experiments were conducted in relatively young animals and may not fully reflect a chronically acquired metabolic disease, like T2D. However, we did deliberately use KS *db/db* mice that are β-cell-deficient and not capable of sufficient compensatory β-cell mass expansion to meet metabolic demand leading to the earlier onset and more profound diabetes. Previous studies reported improved first-phase insulin secretion in overweight patients following co-administration of PYY_{3-36} + GLP-1, yet no additive or synergistic effect compared to GLP-1 alone [46,47]. However, these results were derived from acute exposure of these gut peptides at lower doses and are not necessarily comparable to the beneficial longer-term treatment using Fc-PYY_{3-36} and Fc-GLP-1 which have longer pharmacokinetics. Nonetheless, our data is indicative of enhanced β-cell functional recovery, which was accompanied by increased expression of key genes related to normal β-cell function, in parallel to improved insulin sensitivity and glucose homeostasis. Further mechanistic details of functional β-cell recovery will need to be explored in future studies.

Preclinical rodent studies have demonstrated the weight-lowering potential of GLP-1/PYY_{3-36} co-administration [39], but any pharmacological effects of these combined peptides that are weight-loss independent remain unclear. To this end, we performed experiments in C57BLKS/J *db/db* mice receiving Fc-PYY_{3-36} + Fc-GLP-1 combination treatment and compared to untreated, but weight-matched, animals. Fc-PYY_{3-36} + Fc-GLP-1 combination treatment increased 24 h energy expenditure, VO_2, RER and a trend towards activity relative to weight match controls and restored the more normal circadian pattern of energy expenditure relative to controls during the dark phase (Figure 3C—F). Total activity was reduced in the light phase relative to weight-matched controls. Therefore, some metabolic parameters influenced by Fc-PYY_{3-36} + Fc-GLP-1 are independent of weight loss. However, both GLP-1 and PYY_{3-36} are associated with nausea and emesis [47,48] and consistent with previous reports, we observed a taste aversive effect in monotherapy as well as combination therapy. Of note, conditioned taste aversion to Fc-PYY_{3-36} + Fc-GLP-1 was comparable to the chemotherapeutic cisplatin, indicating aversive feeding behaviour may contribute to some of the pro-metabolic and body weight loss effects Fc-PYY_{3-36} + Fc-GLP-1, but the temporal relationship between dosing and the pathways regulating food intake, body weight, and acute nausea remains to be clarified. As taste aversion was observed with GLP-1 and PYY_{3-36} monotherapies, and more so with the Fc-PYY_{3-36} + Fc-GLP-1 combination, in these preclinical studies at doses that correspond to significant metabolic benefit, further analyses would likely be required to understand whether synergism on efficacy can be uncoupled from tolerability concerns. Lower dose combinations of PYY_{3-36} and GLP-1 have been successful in reducing aversive effects, and dose-titration strategies to mitigate such effects of these incretin classes of therapeutics may be applied [33,43,49]. Nonetheless, the data here suggest that substrate utilization and activity may not explain all the metabolic benefits obtained with Fc-PYY_{3-36} + Fc-GLP-1 combination treatment.

Whether improvement of glucose homeostasis is directly due to weight loss remains a fundamental question in obesity treatment. In diabetic patients undergoing RYGB surgery, rapid improvement in metabolic parameters such as blood glucose and insulin levels occur before any significant weight loss is observed. This suggests that reversal of diabetes by bariatric surgery may be a direct effect, rather than a secondary outcome of weight loss, that in part might be mediated by increases in gut peptide hormone secretion soon after the surgery [50—52]. Here, hyperinsulinaemic-euglycemic clamp studies of Fc-PYY_{3-36} + Fc-GLP-1-treated C57BLKS/J *db/db* mice also demonstrated improved metabolic benefit compared to commensurate weight loss in control animals. Insulin sensitivity during the clamp was significantly improved as evidenced by a 4-fold increase in glucose-infusion rates in Fc-PYY_{3-36} + Fc-GLP-1 combination-treated

C57BLKS/J *db/db* mice, versus weight-matched controls. Both Fc-PYY_{3-36} and Fc-GLP-1 agonist arms contribute to the observed metabolic efficacy of the Fc-PYY_{3-36} + Fc-GLP-1 combination treatment as evidenced by blunted reductions in weight loss and fasting plasma glucose in DIO mice lacking Y2R.

The weight-independent effect of Fc-PYY_{3-36} + Fc-GLP-1 dual agonism in C57BLKS/J *db/db* mice on glucose homeostasis was also observed as significantly increased insulin-stimulated whole-body glucose disposal and suppression of hepatic glucose production relative to weight-matched controls. These improvements in systemic glucose disposal could be attributed to improved insulin sensitivity, leading to enhanced hepatic, BAT, and a potential degree of skeletal muscle, glucose uptake. The fate of skeletal muscle glucose may have been oxidization since insulin-stimulated glycogen synthesis did not increase. Yet, insulin-stimulated hepatic glycogen synthesis was strongly stimulated by Fc-PYY_{3-36} + Fc-GLP-1 combination in C57BLKS/J *db/db* mice, over 10-fold greater than weight-matched controls, implicating a more predominant mechanism for the glucose disposing effects of Fc-PYY_{3-36} + Fc-GLP-1 combination treatment, in line with improved hepatic insulin sensitivity. As neither Y2R nor GLP1R are expressed by skeletal muscle or the liver [53,54], the effect of Fc-PYY_{3-36} + Fc-GLP-1 combination on peripheral and hepatic insulin sensitization must be secondary. The absence of Y2R did not influence whole body or tissue-specific glucose disposal in DIO mice receiving Fc-PYY_{3-36} + Fc-GLP-1 combination treatment, although it did moderate liver-specific glycogen synthesis despite a clear relationship between whole-body glucose disposal, Y2R agonism, and plasma insulin levels during hyperinsulinaemic-euglycemic clamp conditions. However, these Y2RKO mouse studies were limited to much a milder and significantly less insulin resistant DIO model compared to the more severely obese/diabetic C57BLKS/J *db/db* mouse model.

Several studies have revealed how the brain can influence glucose homeostasis in response to afferent input from peripheral signals [55–58]. The hypothalamus, in particular, has historically been associated with the regulation of both liver glycogen content and blood glucose [55]. Recent scientific advances have begun to unravel the neurocircuitry involved in the regulation of blood glucose and energy metabolism [59,60], and the VMH, ARC, DMX, and PVN have all emerged as important metabolic control centres of the CNS. GLP-1 is known to act through GLP-1R expressed on hypothalamic and vagal sensory neurons and the central effects of endogenous brain GLP-1 are well characterized [61–63]. PYY_{3-36} binds to NPY2R and also participates in the hypothalamic control of appetite [9,64]. Given the proposed mode of GLP-1 and PYY_{3-36} dual agonistic action through the hypothalamus, hindbrain, and vagus nerve to regulate energy homeostasis, we speculated whether their combined pharmacology might be mediated through interaction between distinct neural pathways to account for their marked synergistic effect on metabolic homeostasis. An important consideration of this study is the large size of the Fc molecules and their lack of ability to penetrate the blood–brain barrier. Therefore, the neuronal signal transduction observed likely originated in the hypothalamus and or brainstem in locations that lack a blood–brain barrier such as the area postrema and arcuate nucleus. The Fc-PYY_{3-36} + Fc-GLP-1 combination-treatment resulted in robust neuronal activity, as indicated by cFOS activation, in the CeA, NTS, AP, BST, PBN, and PVN regions 4 h post-administration. Activation of these brain regions is consistent with CNS modulation of energy homeostasis [44]. While activation of the AP/NTS then to the PBN and CeA regions is a plausible neuronal pathway [44], the synergistic activation by the combination of GLP-1R and Y2R agonism results in much stronger activation in the PVN and NTS regions of the brain. Furthermore, gene expression analysis revealed a profound increase in the number of regulated genes in the PVN versus the arcuate nucleus or nucleus of the solitary tract suggesting PVN is likely a key early mediator in central activation of metabolic control. By utilizing Y2RKO models, we explored the role of individual receptors and found that synergistic induction of cFos activity in PVN was Y2R-dependent.

Several brain regions showed sustained cFos expression 24 h after Fc-PYY_{3-36} + Fc-GLP-1 combination-treatment demonstrating persistent activity. Notably, the DMX region showed 25-fold greater activation 24 h following Fc-PYY_{3-36} + Fc-GLP-1 co-administration relative to the vehicle. The brainstem dorsal vagal complex integrates hypothalamic inputs and relays the endocrine signal to peripheral organs via vagal efferent fibres resulting in suppression of energy intake and hepatic glucose output [65–67]. As hypothalamic and peripheral Y2R activation decreases food intake by increasing vagal afferent activity, and direct activation of the dorsal vagal complex by PYY_{3-36} appears to increase food intake by attenuating NTS and vagal afferent signalling [68], the mode of PYY_{3-36} action in the brain remains unclear. Most evidence points towards an inhibitory role of PYY_{3-36} in NTS and vagal afferent neurons and one possible mechanism of PYY-GLP-1 synergy could be through disinhibition of GLP-1 induced neuronal activity [44], although has yet to be validated experimentally. More studies are required to characterize specific neuronal populations regulated by individual receptors to better understand the mechanism underlying their synergistic effect. In this regard, it should be noted that aspects of this neuronal circuitry are not only involved in food intake and control of metabolic homeostasis but also taste aversion. As such, future studies should also attempt to tease out the aversive behaviour neuronal network. If this can be separated from those that control satiety and metabolic control, then non-nauseating approaches to treat obesity and T2D might be pursued. Nonetheless, our results indicate that early activation of the PVN and subsequent downstream stimulation of the DMX may represent an initial central activation signal preceding the synergistic homeostatic improvement induced by PYY_{3-36} + GLP-1 co-agonism.

5. CONCLUSIONS

In summary, a therapeutic approach using a combination of long-acting Fc-PYY_{3-36} + Fc-GLP-1 analogues rendered profound weight loss and diabetes remission in two distinct mouse models of obesity-linked T2D, reminiscent of bariatric surgery. The synergistic action of PYY_{3-36} and GLP-1 was recapitulated in the brain via cFOS activation in discrete regions in the hypothalamus and hindbrain which may contribute to the effects on appetite control and metabolic homeostasis. These results also support the hypothesis that alleviating insulin resistance in obesity/T2D improves glucose homeostasis to place less demand on the pancreatic β-cell, and thus endogenous β-cell, functional mass can be sufficiently restored to benefit reversal of T2D progression.

AUTHOR CONTRIBUTIONS

B.B.B., S.O'B., J. H.-S., A.S., D.C.H., L.L., O.P.M., J.L.T., J.S.G., and C.J.R. designed experiments; B.B.B., S.O'B., I.S., J.C.N., P.B., U.R., S.R.S., D.T., A.S., N.B., S.O., S.W., V.H., B.G., P.N., J.N., S.S., R.C.L., J.A., and L.L. conducted experiments, collected, analysed and/or interpreted experimental data; B.B.B., S.S., R.C.L., D.C.H., and C.J.R. drafter the manuscript; B.B.B., S.S., R.C.L., O.P.M, and C.J.R. reviewed and edited the manuscript.

FINANCIAL SUPPORT

These studies were funded by Research and Early Development, Cardiovascular, Renal and Metabolism, BioPharmaceuticals R&D, AstraZeneca. The Vanderbilt Mouse Metabolic Phenotyping Center (MMPC) is supported by NIH/NIDDK funding (DK059637).

ACKNOWLEDGMENTS

The authors thank the Laboratory Animal Resource staff at AstraZeneca for rendering valuable assistance with animal husbandry and care. We would also like to thank the Vanderbilt Mouse Metabolic Phenotyping Center (MMPC) supported by NIH/NIDDK funding (NIH grant no-DK059637).

CONFLICT OF INTEREST

BBB was previously employed by AstraZeneca PLC and Gubra ApS, and is currently employed by PRECISIONscientia; JCN, PB, UR, JH-S, SRS, and DDT are currently employed by Gubra ApS; PB and DDT hold shares in Gubra ApS; SB, IS, SO, SW, BG, PN, JN, SS, RCL, DCH, JSG and CJR are currently employed by AstraZeneca PLC; SB, IS, SO, SW, BG, PN, JN, RCL, DCH, JSG and CJR hold shares in the company; VH was previously employed by AstraZeneca PLC and holds shares in AstraZeneca PLC and Regeneron Pharmaceuticals, LLC.; NB was previously employed by AstraZeneca PLC, is currently employed by Roche and holds shares in Roche; AS was previously employed by AstraZeneca PLC and hold shares in DTXPharma. JLT was previously employed by AstraZeneca PLC, is currently employed by Gilead Sciences, Inc., and holds shares in Gilead Sciences, Inc.

APPENDIX A. SUPPLEMENTARY DATA

Supplementary data to this article can be found online at https://doi.org/10.1016/j.molmet.2021.101392.

REFERENCES

[1] Gadde, K.M., Martin, C.K., Berthoud, H.R., Heymsfield, S.B., Jan 2, 2018. Obesity: pathophysiology and management. Journal of the American College of Cardiology 71(1):69–84.

[2] Kraschnewski, J.L., et al., Nov 2010. Long-term weight loss maintenance in the United States. International Journal of Obesity (London) 34(11):1644–1654.

[3] Madsen, L.R., Baggesen, L.M., Richelsen, B., Thomsen, R.W., Apr 2019. Effect of Roux-en-Y gastric bypass surgery on diabetes remission and complications in individuals with type 2 diabetes: a Danish population-based matched cohort study. Diabetologia 62(4):611–620.

[4] Sjostrom, L., Mar 2013. Review of the key results from the Swedish Obese Subjects (SOS) trial - a prospective controlled intervention study of bariatric surgery. Journal of Internal Medicine 273(3):219–234.

[5] le Roux, C.W., et al., Nov 2007. Gut hormones as mediators of appetite and weight loss after Roux-en-Y gastric bypass. Annals of Surgery 246(5):780–785.

[6] Drucker, D.J., Apr 3, 2018. Mechanisms of action and therapeutic application of glucagon-like peptide-1. Cell Metabolism 27(4):740–756.

[7] Sisley, S., Gutierrez-Aguilar, R., Scott, M., D'Alessio, D.A., Sandoval, D.A., Seeley, R.J., Jun 2014. Neuronal GLP1R mediates liraglutide's anorectic but not glucose-lowering effect. Journal of Clinical Investigation 124(6):2456–2463.

[8] Varin, E.M., et al., Jun 11 2019. Distinct neural sites of GLP-1R expression mediate physiological versus pharmacological control of incretin action. Cell Reports 27(11):3371–3384 e3.

[9] Batterham, R.L., et al., Aug 8 2002. Gut hormone PYY(3-36) physiologically inhibits food intake. Nature 418(6898):650–654.

[10] Abbott, C.R., et al., May 17, 2005. The inhibitory effects of peripheral administration of peptide YY(3-36) and glucagon-like peptide-1 on food intake are attenuated by ablation of the vagal-brainstem-hypothalamic pathway. Brain Research 1044(1):127–131.

[11] Schmidt, J.B., et al., Jun 1 2014. Effects of PYY3-36 and GLP-1 on energy intake, energy expenditure, and appetite in overweight men. American Journal of Physiology. Endocrinology and Metabolism 306(11):E1248–E1256.

[12] Sambrook, J., Russell, D., 2001. Molecular cloning: a laboratory manual (3-volume set).

[13] Butler, R., et al., Apr 2015. Use of the site-specific retargeting jump-in platform cell line to support biologic drug discovery. Journal of Biomolecular Screening 20(4):528–535.

[14] J. Naylor, A. Rossi, and D. C. Hornigold, "Acoustic dispensing preserves the potency of therapeutic peptides throughout the entire drug discovery workflow," , no. 2211-2690 (in eng)(Electronic).

[15] Boland, B., et al., Mar 10, 2019. The PYY/Y2R-deficient mouse responds normally to high-fat diet and gastric bypass surgery. Nutrients 11(3).

[16] Boland, B.B., et al., Jul 2019. Combined loss of GLP-1R and Y2R does not alter the progression of high-fat diet-induced obesity or response to RYGB surgery in mice. Molecular Metabolism 25:64–72.

[17] Boland, B.B., Brown Jr., C., Alarcon, C., Demozay, D., Grimsby, J.S., Rhodes, C.J., Feb 1, 2018. Beta-cell control of insulin production during starvation-refeeding in male rats. Endocrinology 159(2):895–906.

[18] Boland, B.B., et al., Jan 2019. Pancreatic beta-cell rest replenishes insulin secretory capacity and attenuates diabetes in an extreme model of obese type 2 diabetes. Diabetes 68(1):131–140.

[19] Yaekura, K., et al., Mar 14, 2003. Insulin secretory deficiency and glucose intolerance in Rab3A null mice. Journal of Biological Chemistry 278(11):9715–9721.

[20] Alarcon, C., et al., Feb 2016. Pancreatic beta-cell adaptive plasticity in obesity increases insulin production but adversely affects secretory function. Diabetes 65(2):438–450.

[21] Boland, M.L., et al., May 2020. Resolution of NASH and hepatic fibrosis by the GLP-1R/GcgR dual-agonist Cotadutide via modulating mitochondrial function and lipogenesis. Natural Metabolism 2(5):413–431.

[22] Chan, T.M., Exton, J.H., Mar 1976. A rapid method for the determination of glycogen content and radioactivity in small quantities of tissue or isolated hepatocytes. Analytical Biochemistry 71(1):96–105.

[23] Jelsing, J., Galzin, A.M., Guillot, E., Pruniaux, M.P., Larsen, P.J., Vrang, N., Mar 16, 2009. Localization and phenotypic characterization of brainstem neurons activated by rimonabant and WIN55,212-2. Brain Research Bulletin 78(4–5):202–210.

[24] Zhang, C., et al., Jan 15 2020. The dorsomedial hypothalamus and nucleus of the solitary tract as key regulators in a rat model of chronic obesity. Brain Research 1727:146538.

[25] Edgar, R., Domrachev, M., Lash, A.E., Jan 1, 2002. Gene Expression Omnibus: NCBI gene expression and hybridization array data repository. Nucleic Acids Research 30(1):207–210.

[26] Dobin, A., et al., Jan 1, 2013. STAR: ultrafast universal RNA-seq aligner. Bioinformatics 29(1):15–21.

[27] Love, M.I., Huber, W., Anders, S., 2014. Moderated estimation of fold change and dispersion for RNA-seq data with DESeq2. Genome Biology 15(12):550.

[28] Varemo, L., Nielsen, J., Nookaew, I., Apr 2013. Enriching the gene set analysis of genome-wide data by incorporating directionality of gene expression and combining statistical hypotheses and methods. Nucleic Acids Research 41(8):4378–4391.

[29] Haw, R., Stein, L., Jun 2012. Using the reactome database. Current Protocol Bioinformatics Chapter 8. Unit8 7.

[30] Renier, N., Wu, Z., Simon, D.J., Yang, J., Ariel, P., Tessier-Lavigne, M., Nov 6 2014. iDISCO: a simple, rapid method to immunolabel large tissue samples for volume imaging. Cell 159(4):896–910.

[31] Oh, S.W., et al., Apr 10 2014. A mesoscale connectome of the mouse brain. Nature 508(7495):207–214.

[32] Mina, A.I., LeClair, R.A., LeClair, K.B., Cohen, D.E., Lantier, L., Banks, A.S., Oct 2 2018. CalR: a web-based analysis tool for indirect calorimetry experiments. Cell Metabolism 28(4):656–666 e1.

[33] Rangwala, S.M., et al., Apr 2 2019. A long-acting PYY3-36 analog mediates robust anorectic efficacy with minimal emesis in nonhuman primates. Cell Metabolism 29(4):837–843 e5.

[34] Ramracheya, R.D., et al., May 3, 2016. PYY-dependent restoration of impaired insulin and glucagon secretion in type 2 diabetes following roux-en-Y gastric bypass surgery. Cell Reports 15(5):944–950.

[35] Guida, C., et al., Feb 2019. PYY plays a key role in the resolution of diabetes following bariatric surgery in humans. EBioMedicine 40:67–76.

[36] Quail, D.F., Dannenberg, A.J., Mar 2019. The obese adipose tissue microenvironment in cancer development and progression. Nature Reviews Endocrinology 15(3):139–154.

[37] Hall, J.E., do Carmo, J.M., da Silva, A.A., Wang, Z., Hall, M.E., Jun 2019. Obesity, kidney dysfunction and hypertension: mechanistic links. Nature Reviews Nephrology 15(6):367–385.

[38] Talsania, T., Anini, Y., Siu, S., Drucker, D.J., Brubaker, P.L., Sep 2005. Peripheral exendin-4 and peptide YY(3-36) synergistically reduce food intake through different mechanisms in mice. Endocrinology 146(9):3748–3756.

[39] Dalboge, L.S., et al., 2015. A hamster model of diet-induced obesity for preclinical evaluation of anti-obesity, anti-diabetic and lipid modulating agents. PLoS One 10(8):e0135634.

[40] Habib, A.M., Richards, P., Rogers, G.J., Reimann, F., Gribble, F.M., Jun 2013. Co-localisation and secretion of glucagon-like peptide 1 and peptide YY from primary cultured human L cells. Diabetologia 56(6):1413–1416.

[41] Chepurny, O.G., et al., Feb 28 2018. Chimeric peptide EP45 as a dual agonist at GLP-1 and NPY2R receptors. Scientific Reports 8(1):3749.

[42] Field, B.C., et al., Jul 2010. PYY3-36 and oxyntomodulin can be additive in their effect on food intake in overweight and obese humans. Diabetes 59(7):1635–1639.

[43] De Silva, A., et al., Nov 2 2011. The gut hormones PYY 3-36 and GLP-1 7-36 amide reduce food intake and modulate brain activity in appetite centers in humans. Cell Metabolism 14(5):700–706.

[44] Kjaergaard, M., Salinas, C.B.G., Rehfeld, J.F., Secher, A., Raun, K., Wulff, B.S., Feb 2019. PYY(3-36) and exendin-4 reduce food intake and activate neuronal circuits in a synergistic manner in mice. Neuropeptides 73:89–95.

[45] Puff, R., et al., May 2011. Reduced proliferation and a high apoptotic frequency of pancreatic beta cells contribute to genetically-determined diabetes susceptibility of db/db BKS mice. Hormone and Metabolic Research 43(5):306–311.

[46] Tan, T.M., et al., Nov 2014. Combination of peptide YY3-36 with GLP-1(7-36) amide causes an increase in first-phase insulin secretion after IV glucose. The Journal of Cinical Endocrinology and Metabolism 99(11):E2317–E2324.

[47] Degen, L., et al., Nov 2005. Effect of peptide YY3-36 on food intake in humans. Gastroenterology 129(5):1430–1436.

[48] Bettge, K., Kahle, M., Abd El Aziz, M.S., Meier, J.J., Nauck, M.A., Mar 2017. Occurrence of nausea, vomiting and diarrhoea reported as adverse events in clinical trials studying glucagon-like peptide-1 receptor agonists: a systematic analysis of published clinical trials. Diabetes, Obesity and Metabolism 19(3):336–347.

[49] Neary, N.M., et al., Dec 2005. Peptide YY3-36 and glucagon-like peptide-17-36 inhibit food intake additively. Endocrinology 146(12):5120–5127.

[50] Dirksen, C., et al., Dec 2013. Exaggerated release and preserved insulinotropic action of glucagon-like peptide-1 underlie insulin hypersecretion in glucose-tolerant individuals after Roux-en-Y gastric bypass. Diabetologia 56(12):2679–2687.

[51] Guidone, C., et al., Jul 2006. Mechanisms of recovery from type 2 diabetes after malabsorptive bariatric surgery. Diabetes 55(7):2025–2031.

[52] Martinussen, C., et al., Mar 15 2015. Immediate enhancement of first-phase insulin secretion and unchanged glucose effectiveness in patients with type 2 diabetes after Roux-en-Y gastric bypass. American Journal of Physiology. Endocrinology and Metabolism 308(6):E535–E544.

[53] Dai, W., et al., Jul 1 2019. Expression of neuropeptide Y is increased in an activated human HSC cell line. Scientific Reports 9(1):9500.

[54] Panjwani, N., et al., Jan 2013. GLP-1 receptor activation indirectly reduces hepatic lipid accumulation but does not attenuate development of atherosclerosis in diabetic male ApoE(-/-) mice. Endocrinology 154(1):127–139.

[55] Shimazu, T., Jan 1996. Innervation of the liver and glucoregulation: roles of the hypothalamus and autonomic nerves. Nutrition 12(1):65–66.

[56] Bentsen, M.A., Mirzadeh, Z., Schwartz, M.W., Jan 8, 2019. Revisiting how the brain senses glucose-and why. Cell Metabolism 29(1):11–17.

[57] Myers Jr., M.G., Olson, D.P., Nov 15 2012. Central nervous system control of metabolism. Nature 491(7424):357–363.

[58] Ruud, J., Steculorum, S.M., Bruning, J.C., May 4 2017. Neuronal control of peripheral insulin sensitivity and glucose metabolism. Nature Communications 8:15259.

[59] Klockener, T., et al., Jun 5 2011. High-fat feeding promotes obesity via insulin receptor/PI3K-dependent inhibition of SF-1 VMH neurons. Nature Neuroscience 14(7):911–918.

[60] Meek, T.H., et al., Apr 5 2016. Functional identification of a neurocircuit regulating blood glucose. Proceedings of the National Academy of Sciences of the U S A 113(14):E2073–E2082.

[61] Lopez-Ferreras, L., et al., May 2018. Lateral hypothalamic GLP-1 receptors are critical for the control of food reinforcement, ingestive behavior and body weight. Molecular Psychiatry 23(5):1157–1168.

[62] Kanoski, S.E., Fortin, S.M., Arnold, M., Grill, H.J., Hayes, M.R., Aug 2011. Peripheral and central GLP-1 receptor populations mediate the anorectic effects of peripherally administered GLP-1 receptor agonists, liraglutide and exendin-4. Endocrinology 152(8):3103–3112.

[63] Vahl, T.P., et al., Oct 2007. Glucagon-like peptide-1 (GLP-1) receptors expressed on nerve terminals in the portal vein mediate the effects of endogenous GLP-1 on glucose tolerance in rats. Endocrinology 148(10):4965–4973.

[64] Broberger, C., Landry, M., Wong, H., Walsh, J.N., Hokfelt, T., Dec 1997. Subtypes Y1 and Y2 of the neuropeptide Y receptor are respectively expressed in pro-opiomelanocortin- and neuropeptide-Y-containing neurons of the rat hypothalamic arcuate nucleus. Neuroendocrinology 66(6):393–408.

[65] Grill, H.J., Hayes, M.R., Sep 5, 2012. Hindbrain neurons as an essential hub in the neuroanatomically distributed control of energy balance. Cell Metabolism 16(3):296–309.

[66] Lam, C.K., Chari, M., Rutter, G.A., Lam, T.K., Jan 2011. Hypothalamic nutrient sensing activates a forebrain-hindbrain neuronal circuit to regulate glucose production in vivo. Diabetes 60(1):107–113.

[67] Rossi, J., et al., Feb 2, 2011. Melanocortin-4 receptors expressed by cholinergic neurons regulate energy balance and glucose homeostasis. Cell Metabolism 13(2):195–204.

[68] Huston, N.J., Brenner, L.A., Taylor, Z.C., Ritter, R.C., Apr 1, 2019. NPY2 receptor activation in the dorsal vagal complex increases food intake and attenuates CCK-induced satiation in male rats. American Journal of Physiology - Regulatory, Integrative and Comparative Physiology 316(4):R406–R416.

